The Rab11-family interacting proteins reveal selective interaction of mammalian recycling endosomes with the *Toxoplasma* parasitophorous vacuole in a Rab11- and Arf6-dependent manner

Eric J. Hartman[†], Beejan Asady[†], Julia D. Romano[‡,*], and Isabelle Coppens[‡,*]
Department of Molecular Microbiology and Immunology, Johns Hopkins School of Public Health, Baltimore, MD 21205

ABSTRACT **After mammalian cell invasion, the parasite *Toxoplasma* multiplies in a self-made membrane-bound compartment, the parasitophorous vacuole (PV). We previously showed that *Toxoplasma* interacts with many host cell organelles, especially from recycling pathways, and sequestrates Rab11A and Rab11B vesicles into the PV. Here, we examine the specificity of host Rab11 vesicle interaction with the PV by focusing on the recruitment of subpopulations of Rab11 vesicles characterized by different effectors, for example, Rab11-family interacting roteins (FIPs) or Arf6. Our quantitative microscopic analysis illustrates the presence of intra-PV vesicles with FIPs from class I (FIP1C, FIP2, FIP5) and class II (FIP3, FIP4) but to various degrees. The intra-PV delivery of vesicles with class I, but not class II, FIPs is dependent on Rab11 binding. Cell depletion of Rab11A results in a significant decrease in intra-PV FIP5, but not FIP3 vesicles. Class II FIPs also bind to Arf6, and we observe vesicles associated with FIP3-Rab11A or FIP3-Arf6 complexes concomitantly within the PV. Abolishing FIP3 binding to both Rab11 and Arf6 reduces the number of intra-PV FIP3 vesicles. These data point to a selective process of mammalian Rab11 vesicle recognition and scavenging mediated by *Toxoplasma*, suggesting that specific parasite PV proteins may be involved in these processes.**

Monitoring Editor
Dominique Soldati-Favre
University of Geneva

Received: Jun 2, 2021
Revised: Feb 3, 2022
Accepted: Mar 01, 2022

INTRODUCTION

The small monomeric Rab GTPases belong to the Ras superfamily and are master regulators of vesicular trafficking and signaling pathways (Chavrier and Goud, 1999). Many intracellular pathogens hijack the host Rab membrane trafficking machinery to thrive in a hostile environment. Among protozoan parasites, Apicomplexa are obligate intracellular microbes that invade mammalian cells by creating a protective, nonfusogenic membrane-bound compartment, the parasitophorous vacuole (PV). Recent evidence demonstrates that apicomplexan parasites manipulate several mammalian Rab vesicle trafficking pathways to scavenge nutrients or to exploit the functions of Rab GTPase proteins for immune evasion (reviewed in Coppens and Romano, 2020). The apicomplexan *Toxoplasma gondii*, the etiologic agent of toxoplasmosis, diverts many host Rab vesicles to the PV and sequesters some of them in the PV lumen through deep invaginations of the PV membrane (Romano *et al.*, 2013, 2017; Nolan *et al.*, 2017; Coppens and Romano, 2020). Host Rab vesicles from the recycling and secretory (anterograde) pathways are detected in the vast majority of the *Toxoplasma* PV (Romano *et al.*, 2017). *Toxoplasma* predominantly hijacks the GTP-bound form of Rab proteins to intercept vesicular traffic, at least as a means for lipid procuration. Indeed, the parasite salvages sphingolipids manufactured in the host endoplasmic reticulum/Golgi and accesses these lipids through the interception of Rab14, Rab30, and Rab43 vesicles (Romano *et al.*, 2013).

This article was published online ahead of print in MBoC in Press (http://www.molbiolcell.org/cgi/doi/10.1091/mbc.E21-06-0284) on March 11, 2022.

[†]Equally first authors.

[‡]Equally senior authors.

*Address correspondence to: Julia D. Romano (jromano2@jhu.edu); Isabelle Coppens (icoppens@jhsph.edu).

Abbreviations used: ABD, Arf6-binding domain; ERC, endocytic recycling compartment; FIP, Rab11-family interacting protein; IVN, intravacuolar network; PV, parasitophorous vacuole; RBD, Rab11-binding domain; RE, recycling endosomes; RFP-Tg, RFP-expressing *Toxoplasma*; TfR, transferrin receptor.

The Rab11 proteins, comprising Rab11A, Rab11B, and Rab11C/Rab25, localize to different cellular compartments (e.g., the *trans*-Golgi network [TGN], *post*-Golgi vesicles, and/or pericentriolar recycling endosomes [RE]), indicating division of selective functions between the three subfamily members (Grant and Donaldson, 2009; Welz *et al.*, 2014). Broadly, Rab11 proteins regulate the recycling of many receptors and adhesion proteins to the cell surface and play roles in various cellular functions, including ciliogenesis, cytokinesis, neuritogenesis, and oogenesis (Kelly *et al.*, 2012). In particular, Rab11A is involved in phagocytosis, synaptic function, and cell migration and in the delivery of vesicles to the cleavage furrow/midbody during cell division (Cox *et al.*, 2000; Yoon *et al.*, 2005; Caswell *et al.*, 2008; Wang *et al.*, 2008; Kelly *et al.*, 2011; Horgan *et al.*, 2012). Rab11B is essential for the recycling/trafficking of the transferrin receptor, the epithelial sodium channel, the cystic fibrosis transmembrane conductance regulator, and vacuolar type H^+-ATPases and for calcium-induced exocytotic events (Schlierf *et al.*, 2000; Khvotchev *et al.*, 2003; Silvis *et al.*, 2009; Sugawara *et al.*, 2009; Best *et al.*, 2011; Butterworth *et al.*, 2012). Associated with apical RE, Rab11C/Rab25 regulates the processes of transcytosis and plasma membrane recycling (Casanova *et al.*, 1999). Abnormal Rab11 activity (deficiency or overexpression) has been shown to be implicated in the progression of numerous human diseases (e.g., cancers, neurodegeneration, diabetes; Bhuin and Roy, 2015). Mammalian Rab11 vesicles are largely diverted by *Toxoplasma*, with 89% and 100% of PV containing Rab11A and Rab11B vesicles, respectively (Romano *et al.*, 2017).

In this study, we sought to address the specificity of host Rab11 vesicle interaction with the PV of *Toxoplasma*. In particular, we wanted to examine whether the parasite indiscriminately hijacks any host Rab11A or Rab11B vesicles regardless of composition or localization in infected cells or whether the parasite selectively recognizes subpopulations of Rab11A or Rab11B vesicles associated with specific effectors. Rab11 proteins interact with different effectors depending on their GTP/GDP status that is regulated by guanine nucleotide exchange factors (GEF) and GTPase-activating proteins (GAP) (Zerial and McBride, 2001). In the active state, Rab11 proteins bind to effector proteins termed the Rab11-family interacting proteins (FIPs), allowing Rab11 proteins to recruit cellular motor proteins (Horgan and McCaffrey, 2009). FIPs interact indiscriminately with GTP-bound Rab11A and Rab11B via a conserved 20-amino-acid C-terminal domain, named the Rab11-binding domain (RBD) (Junutula *et al.*, 2004; Eathiraj *et al.*, 2006; Jagoe *et al.*, 2006; Horgan and McCaffrey, 2009). Mutations introduced into the RBD of FIP disrupt binding to Rab11 and therefore alter the localization of the FIP (Meyers and Prekeris, 2002; Junutula *et al.*, 2004; Lindsay and McCaffrey 2004a; Fielding *et al.*, 2005; Wilson *et al.*, 2005; Jagoe *et al.*, 2006; Horgan *et al.*, 2007). In addition to the RBD, each FIP has an α-helical coiled-coil structure mediating FIP homodimerization necessary to execute FIP cellular functions (Wei *et al.*, 2006; Horgan *et al.*, 2007). FIPs form heterotetrameric complexes with Rab11 composed of two Rab11 and two FIP molecules.

Based on their primary structure, FIPs are subcategorized into class I, with FIP1C (*alias* Rab-coupling protein), FIP2 and FIP5 (*alias* Rip11, Gaf-1/Gaf-1b, pp75 or gamma-SNAP Associated Factor), and class II, with FIP3 (*alias* Arfophilin or Eferin) and FIP4 (*alias* Arfophilin-2). class I FIPs have a phospholipid-binding C2-domain that targets the Rab11-FIP complexes to docking sites on the plasma membrane selectively enriched in phosphatidylinositol-3,4,5-trisphosphate and phosphatidic acid, two lipids required for fusion (Prekeris *et al.*, 2000; Lindsay *et al.*, 2002; Fan *et al.*, 2004; Lindsay and McCaffrey, 2004b). Class II FIPs contain a calcium-binding EF-Hand domain that functions in targeting new membranes to the cleavage furrow for the completion of cytokinesis and is necessary for the structural integrity of the pericentrosomal endocytic recycling compartment (ERC) (Horgan *et al.*, 2007). The ERC is constituted of a large complex of heterogeneous subsets of RE, tubular RE, and small transport intermediates (Maxfield and McGraw, 2004).

FIP3 and FIP4 also bind members of the Arf GTPase family, most notably Arf6, on an Arf-binding domain (ABD) in the C-terminal region that is distinct from the RBD (Shin *et al.*, 1999; Fielding *et al.*, 2005; Shiba *et al.*, 2006). Arf6 forms ternary complexes with Rab11 and FIP3 or FIP4 and mediates the recruitment of Rab11-FIP3 and Rab11-FIP4 to the cleavage furrow (Wallace *et al.*, 2002; Horgan *et al.*, 2004; Wilson *et al.*, 2005; Fielding *et al.*, 2005). Deletion of the ABD from FIP3 in neurons leads to defects in Arf6-regulated delivery of endosome recycling pathways, such as aberrant cytoplasmic retention of N-cadherin and syntaxin 12. The resulting phenotype is impairment in neuron migration, which reveals the importance of Arf6-FIP endosomal trafficking pathways (Hara *et al.*, 2016).

On the basis of the composition of Rab11 complexes, we devised quantitative microscopy-based assays to assess the distribution of mammalian vesicles with FIP (FIP1C, FIP2, FIP3, FIP4, and FIP5) and Arf6 in *Toxoplasma*-infected cells, with the anticipation that subpopulations of Rab11 vesicles would be selectively recognized at the PV membrane and internalized into the vacuole. We also examined the contribution of Rab11 and Arf6 binding to the internalization of FIP-associated vesicles through mutations of the RBD and/or ABD of FIP or through Rab11A down-regulation in mammalian cells. Our in vitro assays reveal differential interception and PV internalization of host RE based on effector and Rab11 complex composition.

RESULTS

Mammalian Rab11 vesicle subpopulations with either class I or class II FIPs are associated with the PV of *Toxoplasma*

In mammalian cells, the intravacuolar parasite *Toxoplasma* intercepts the trafficking of host recycling vesicles (Romano *et al.*, 2017). The recruitment of host Rab11 vesicles at the PV was monitored by two assays: transfection of mammalian cells with green fluorescent protein (GFP)-Rab11 plasmids before infection or immunofluorescence assays (IFA) in infected cells using antibodies recognizing Rab11 proteins. In HeLa cells transiently expressing GFP-Rab11B, the fluorescent signal was dispersed throughout the cytoplasm in uninfected cells but observed in the vicinity of the PV upon infection (Figure 1Aa). Several GFP foci were also detected within the PV (delineated by TgGRA7 staining), as illustrated on the orthogonal views of two PV. Similarly, in HeLa cells expressing GFP-Rab11A, the perinuclear fluorescent signal in uninfected cells redistributed around the PV upon infection, with GFP-Rab11A foci also observed in the PV lumen (Figure 1Ab). An IFA using an antibody that recognizes Rab11 isoforms in infected cells gave a punctate fluorescent pattern surrounding the PV compared with the vesicular staining uniformly distributed in the cytoplasm in uninfected cells (Figure 1Ba). Examination of the PV interior reveals the presence of several Rab11 vesicles in the middle of the rosette-like structure formed by replicating *Toxoplasma*. In infected Vero cells stably expressing GFP-Rab11A, GFP-Rab11A foci were detected within the PV (Romano *et al.*, 2017) and quantification of GFP-Rab11A foci reveals an average of 8.5 per PV (Figure 1Bb). We immunostained infected Vero cells stably expressing GFP-Rab11A with a specific antibody against Rab11A, and the fluorescent signals for anti-Rab11A antibody and GFP showed significant colocalization in the host cytosol and close to the plasma membrane (Figure 1Bc). In infected HeLa

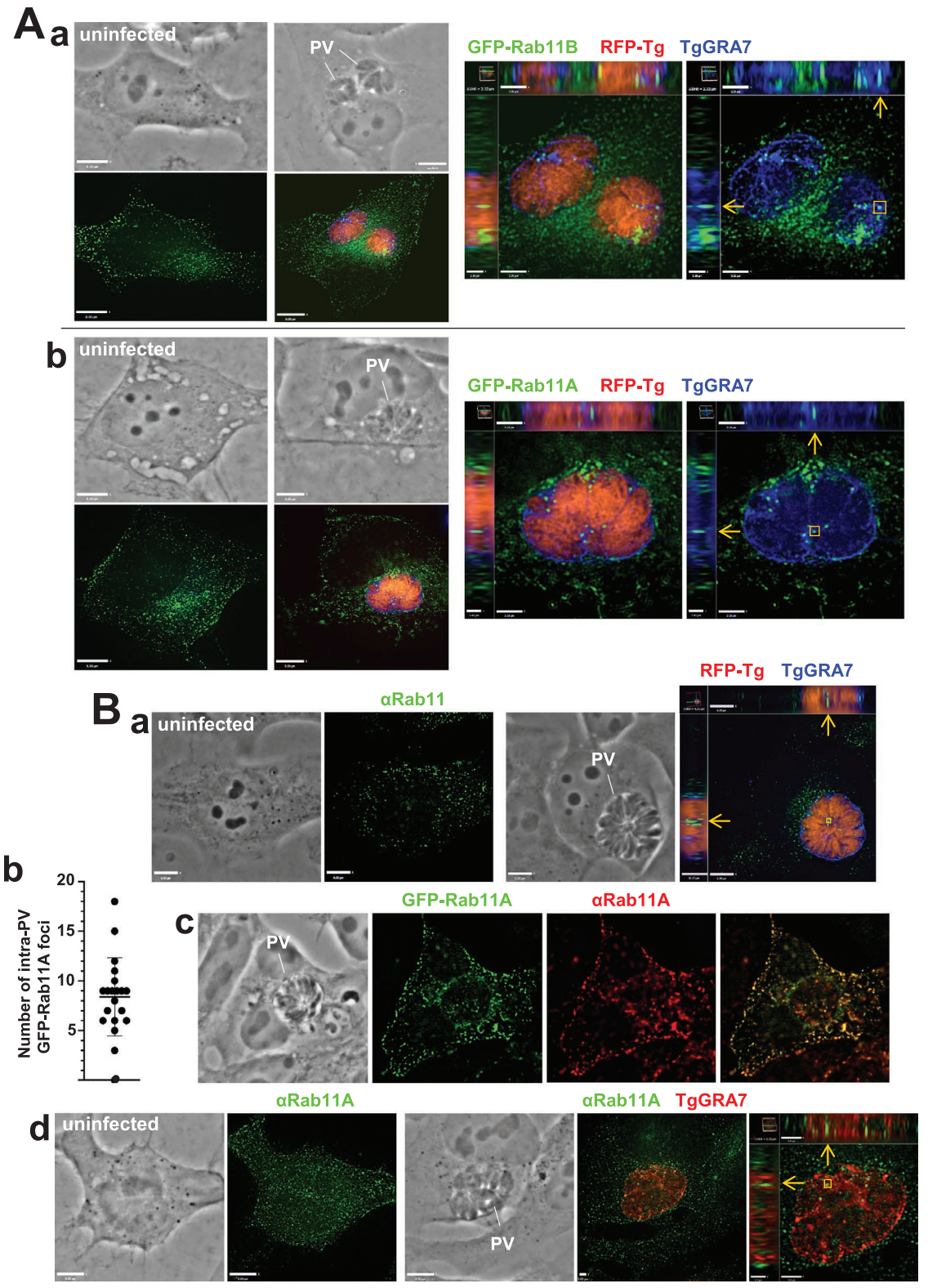

FIGURE 1: Distribution of mammalian Rab11 vesicles in *Toxoplasma*-infected cells. (A) Fluorescence microscopy of HeLa cells transiently expressing GFP-Rab11B (panel a) or GFP-Rab11A (panel b) uninfected or infected with red fluorescent protein (RFP)-expressing *Toxoplasma* (RFP-Tg) for 24 h before immunostaining with anti-TgGRA7 antibody. (B) Fluorescence microscopy of HeLa cells uninfected or infected with *Toxoplasma* for 24 h before immunostaining with anti-Rab11 and anti-TgGRA7 antibodies (panel a); in Vero cells stably expressing Rab11A, enumeration of intra-PV GFP-Rab11A vesicles (panel b); fluorescence microscopy of infected GFP-Rab11A–expressing Vero cells immunostained with anti-Rab11A antibody, showing fluorescent signal overlap (panel c); HeLa cells uninfected or infected for 24 h before immunostaining with anti-Rab11A and anti-TgGRA7 antibodies (panel d). For all images, individual *z*-slices and orthogonal views spanning the PV interior are shown. Examples of intra-PV Rab11 foci are framed (yellow squares).

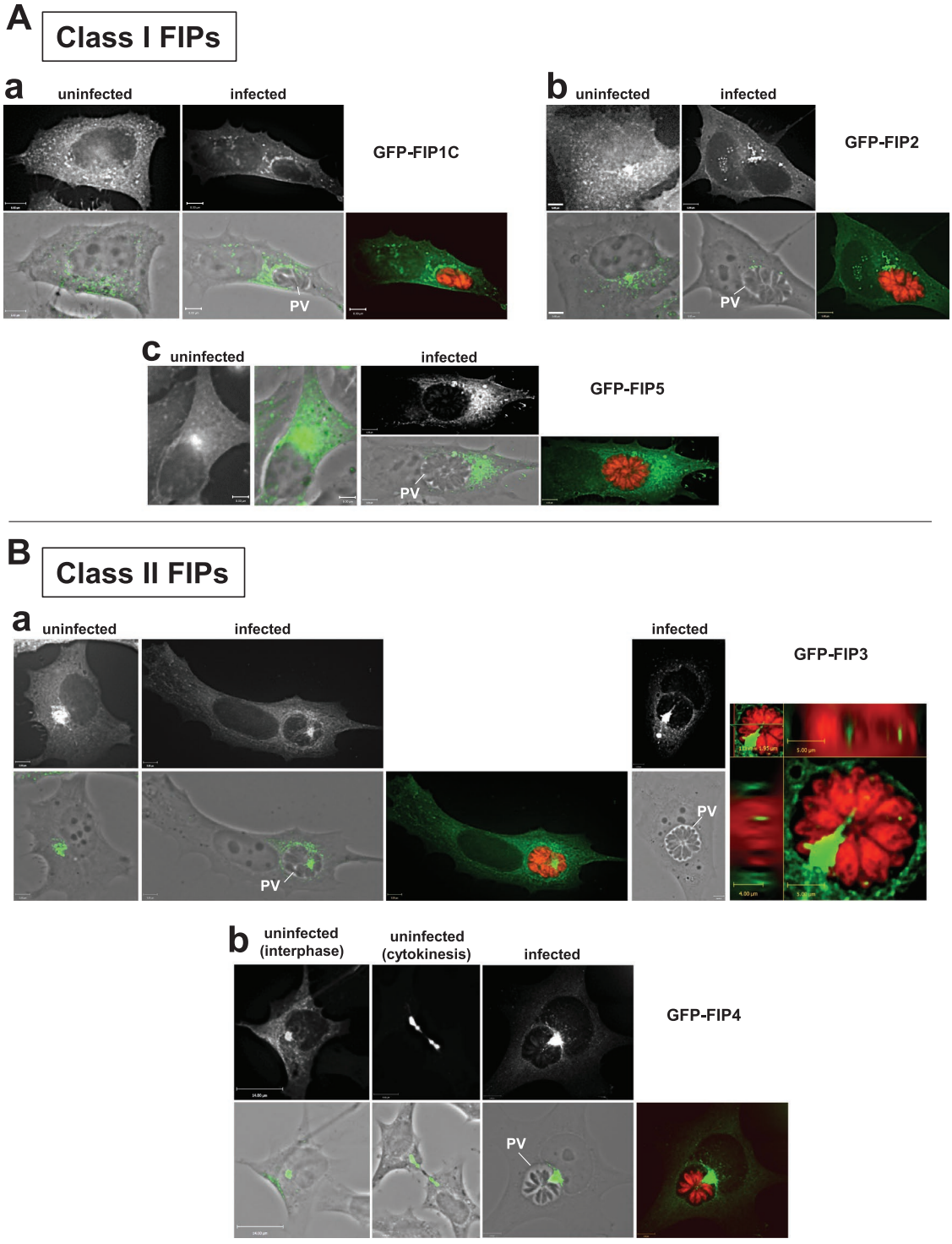

FIGURE 2: Distribution of mammalian vesicles containing FIP from classes I and II in *Toxoplasma*-infected cells. (A, B) Fluorescence microscopy of HeLa cells transfected with class I FIPs (GFP-FIP1C, GFP-FIP2, or GFP-FIP5 in A) and class II FIPs (GFP-FIP3 or GFP-FIP4 in B) uninfected or infected with RFP-Tg for 24 h. Phase contrast overlaid with the GFP-FIP signal is shown as well as the GFP-FIP alone and with the RFP signal.

cells, the antibody signal was also observed within the vacuole (Figure 1Bd). Thus, these IFA data confirm our transfection data on cells ectopically expressing Rab11 constructs and highlight the sequestration of host Rab11 vesicles into the PV.

Next, we wanted to examine whether *Toxoplasma* selectively recruits subpopulations of mammalian Rab11 vesicles by focusing on specific Rab11 effectors that govern localization and recycling function. We transiently transfected HeLa cells with a plasmid containing a FIP from class I (FIP1C, FIP2, FIP5) or class II (FIP3, FIP4) fused N-terminally with GFP. Posttransfection, cells were infected with RFP-expressing *Toxoplasma* (RFP-Tg) for 24 h. In uninfected HeLa cells, GFP-FIP1C exhibited a wide distribution in the cytoplasm, demarcating tubular structures preferentially distributed at the perinuclear region (Figure 2Aa). In infected cells, GFP-FIP1C structures were

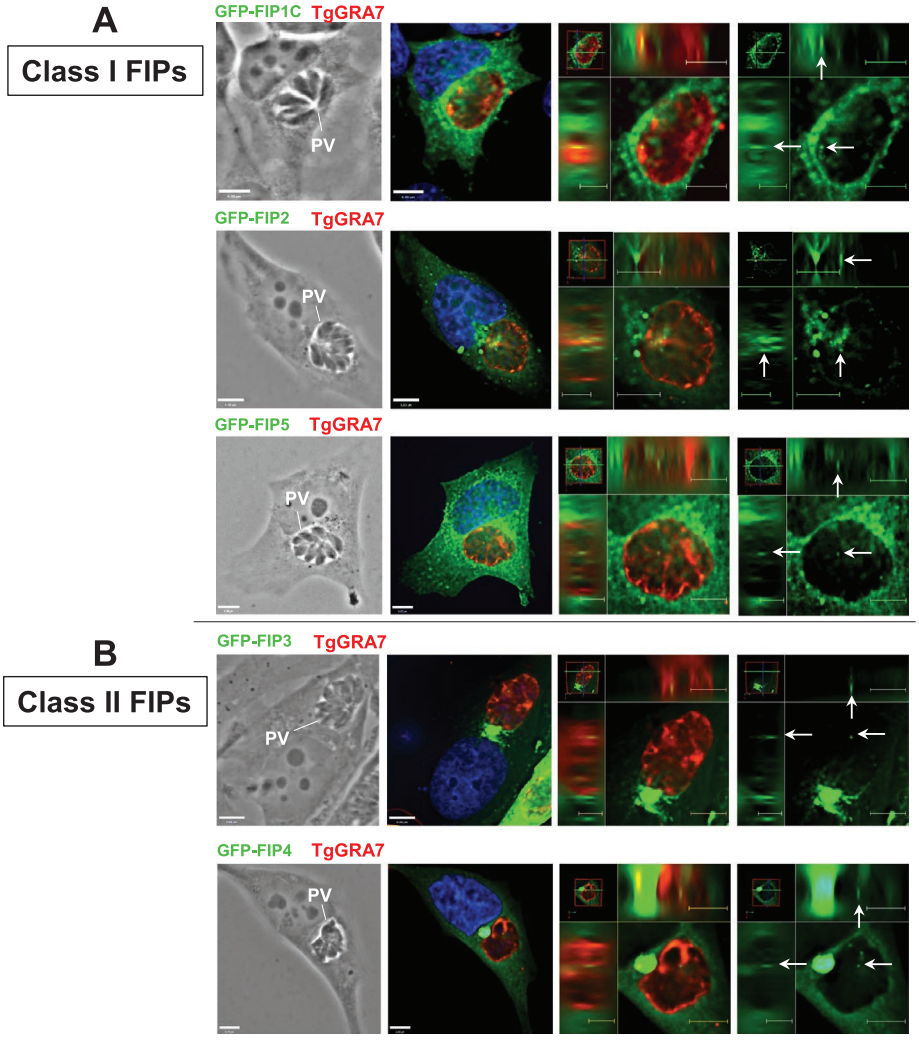

C

FIP	Class	% PV with GFP-FIP foci (# of PV)	
		WT	Δgra2Δgra6
FIP1C	I	12% (25)	0% (22)
FIP2	I	57% (21)	0% (23)
FIP5	I	52% (21)	5% (22)
FIP3	II	88% (24)	0% (20)
FIP4	II	50% (24)	8% (24)

FIGURE 3: Distribution of mammalian vesicles containing FIP from classes I and II within the *Toxoplasma* PV. (A, B) Fluorescence microscopy of HeLa cells transfected with GFP-FIP (class I in A: GFP-FIP1C, GFP-FIP2, or GFP-FIP5; class II in B: GFP-FIP3 or GFP-FIP4) uninfected or infected with RFP-Tg for 24 h before immunostaining with anti-TgGRA7 antibody. DAPI in blue. For all images, individual *z*-slices and orthogonal views are shown. Arrows show intra-PV GFP-FIP foci. (C) Quantification of the internalization of class I and II FIP vesicles within the *Toxoplasma* PV. Percent of PV with intra-PV foci was assessed based on PV viewed in A and B. Negative controls include PV from Δgra2Δgra6 mutants impaired in host vesicle internalization.

observed concentrated around the PV. In uninfected cells expressing GFP-FIP2, the fluorescent pattern was similar to that of GFP-FIP1C, and upon infection, it also delocalized to the PV (Figure 2Ab). Compared to the GFP-FIP1C and GFP-FIP2, the fluorescent signal of GFP-FIP5 was predominantly centralized in the juxtanuclear region of uninfected cells (Figure 2Ac). Following infection, GFP-FIP5 localization was more prominent at the PV than at the host nucleus.

Next, we compared the localizations of class II FIPs (FIP3, FIP4) in uninfected and infected cells. It has been reported that exogenous expression of FIP3 or FIP4, which localize to the ERC, induces alteration in the morphology of the ERC as this organelle condenses around the microtubule-organizing center (MTOC) at the pericentrosomal region of cells during interphase (Wallace *et al.*, 2002; Horgan *et al.*, 2004). During cytokinesis, FIP3 and FIP4 vesicles move to the cleavage furrow, a process also amplified upon FIP3 and FIP4 overexpression (Wallace *et al.*, 2002; Horgan *et al.*, 2004; Fielding *et al.*, 2005; Wilson *et al.*, 2005). In HeLa cells expressing GFP-FIP3 or GFP-FIP4, we confirmed an intense fluorescent staining at the ERC and the cleavage furrow in nondividing and mitotic cells, respectively (Figure 2B, a and b). Upon *Toxoplasma* infection, the GFP-FIP3- or GFP-FIP4–positive ERC was delocalized from its perinuclear location and associated with the PV.

Mammalian Rab11 vesicle subpopulations, defined by FIPs, are selectively internalized into the *Toxoplasma* PV based on the percent of PV containing vesicles

Aggregation at the *Toxoplasma* PV of host vesicles marked with FIP1C, FIP2, FIP5, FIP3, or FIP4 may precede the internalization of these vesicles into the PV. In infected HeLa cells expressing GFP-FIP for each FIP, the intra-PV localization of GFP-FIP foci was monitored by fluorescence microscopy by collecting a series of optical z-sections throughout the PV defined by TgGRA7 immunostaining. GFP-FIP foci were observed within the PV for all the FIP constructs from class I (Figure 3A) and class II (Figure 3B). Detection of intra-PV FIP vesicles was confirmed by IFA for endogenous FIP5 and FIP3 using antibodies against these proteins (Supplemental Figure S1).

The percentages of PV positive for intra-PV GFP-FIP foci were different among the FIPs; the lowest PV percentage was measured for FIP1C (12%) and the highest for FIP3 (88%) (Figure 3C). Approximately 50% of PV contained FIP2, FIP5, or FIP4 vesicles. The interior of the PV is characterized by the presence of an entangled network of membranous tubules (~30 nm diameter), named the intravacuolar network (IVN) (Sibley *et al.*, 1995). Previously, we illustrated by electron microscopy (EM) the attachment of IVN tubules to the PV membrane, which provide "open gates" for the entry of host material into the PV, and we detected host organelles, including Rab vesicles within the tubules forming the IVN (Romano *et al.*, 2017). A *Toxoplasma* mutant lacking two IVN-localized proteins involved in IVN biogenesis (TgGRA2 and TgGRA6) shows complete disruption of this network, which is reduced to loose

membrane whorls (Mercier *et al.*, 2002) and is impaired in host organelle sequestration into the PV (Romano *et al.*, 2017). This mutant was used as a negative control in our assays, and as expected, 0–8% of PV contained GFP foci. Even for PV with a GFP signal, fluorescent puncta for FIP5 or FIP4 were very tiny in the PV of Δgra2Δgra6 parasites, compared with wild type (WT) (Supplemental Figure S2).

PV sequestration of vesicles marked with class I FIP but not class II FIP requires the formation of Rab11-FIP complexes

FIP proteins play a role in targeting Rab11 to different endocytic compartments by competing with each other for Rab11 binding (Meyers and Prekeris, 2002). Next, we examined whether the recruitment of FIP-associated vesicles at the PV and their internalization into the vacuole required the presence of Rab11 bound to FIP. Substitution of the hydrophobic isoleucine residue to a negatively charged glutamic acid within the RBD of FIP1C (I621E mutation), FIP2 (I481E mutation), FIP5(I630E mutation), and FIP3 (I738E mutation) or replacement of the tripeptidic sequence tyrosine–methionine–aspartate by three alanine residues in the RBD of FIP4 (YMD617-619AAA) totally abrogates FIP binding to Rab11, and the distribution of FIP-RBD mutant vesicles is grossly altered in mammalian cells (Meyers and Prekeris, 2002; Junutula *et al.*, 2004; Lindsay and McCaffrey, 2004a; Fielding *et al.*, 2005; Wilson *et al.*, 2005; Jagoe *et al.*, 2006; Horgan *et al.*, 2007). We transiently transfected HeLa cells with plasmids containing each FIP-RBD mutant fused to GFP, and the GFP signal was predominantly dispersed throughout the cell, with a noticeable loss of pericentrosomal ERC staining for FIP3 and FIP4 (Figure 4, A and B). Following a 24 h infection of transfected cells, fluorescent perivacuolar labeling was observed, suggesting the ability of the parasite to attract FIP-RBD mutant vesicles, though to a lesser extent for FIP2-RBD. Interestingly, many PV in HeLa cells expressing the mutants FIP3-RBD and FIP4-RBD contained numerous GFP foci (Figure 4B). In contrast, no intra-PV GFP signal was detected for the class I FIP-RBD mutants (Figure 5A). For the class II mutants, all PV were positive for FIP4-RBD mutant vesicles and three-fourths of PV for FIP3-RBD mutant vesicles (Figure 5B). No GFP foci of FIP3-RBD and FIP4-RBD mutants were spotted in the PV of Δgra2Δgra6 parasites, as expected (Supplemental Figure S2). The intra-PV GFP-FIP foci were counted either in all PV (including PV with no internalization events as zero foci; Figure 6A) or solely in positive PV (corresponding to PV containing at least one foci; Figure 6B) in infected HeLa cells expressing FIPs-WT and FIPs-RBD mutants. The greatest number of intra-PV vesicles was scored for the class II FIP mutants, with an average number of 7.4 FIP3-RBD foci per positive PV and 6.3 FIP4-RBD foci per positive PV, which was significantly greater than the number of WT FIP3 or FIP4 intra-PV vesicles (Figure 6B).

We conducted immunoelectron microscopy studies on HeLa cells expressing GFP-FIP3 or the GFP-FIP3-RBD mutant using anti-GFP antibody to scrutinize the GFP-positive vesicles around and inside the PV. In uninfected GFP-FIP3–expressing cells, gold particles were detected on the membranes of several vesicles and tubules in the cytoplasm (Figure 7Aa). In infected transfected cells, a noticeable gathering of labeled structures was observed around the PV (Figure 7Ab). Gold particles were also present on intra-PV vesicles (Figure 7Ac; Supplemental Figure S3), and high-magnification observations reveals the gold staining on vesicular membranes (Figure 7Ad). In HeLa cells expressing GFP-FIP3-RBD, the gold particle staining was more diffuse throughout the cell and partly associated with vesicles (Figure 7Ba). Similar to the GFP-FIP3 WT signal in infected cells, gold particles were observed in close proximity to the PV (Figure 7B b); numerous labeled vesicles were detected in the PV lumen (Figure 7B, c and c′; Supplemental Figure S4) and membrane-associated on vesicles inside IVN tubules (Figure 7Bd). These data illustrate that the GFP-FIP3 foci (WT and RBD) are associated with vesicles internalized into the PV.

Jointly, these observations illustrate a striking difference between the two FIP classes regarding FIP vesicle internalization into the PV as the formation of Rab11-FIP complexes is required for class I but is dispensable for class II and even unfavorable based on the greater number of FIP3- and FIP4-RBD mutant vesicles detected in the PV.

The PV contains mammalian vesicles marked with Rab11A, FIP3, or Rab11A-FIP3 complexes

The internalization of FIP3-positive vesicles into the PV independently of Rab11 led us to investigate the percentage of intra-PV Rab11A vesicles that are associated with FIP3. Transfected HeLa cells expressing GFP-FIP3 were immunolabeled with anti-Rab11A antibody to assess the colocalization of FIP3 and endogenous Rab11A proteins on vesicles. Expression of FIP3 in HeLa cells resulted in the congregation of Rab11A vesicles on pericentrosomal ERC with FIP3 (Figure 8Aa) as compared with nontransfected cells, where Rab11A vesicles (detected by immunostaining) were distributed throughout the cell with partial concentration at the ERC (Figure 1A). The GFP-FIP3 signal was also distributed on ERC tubular extensions that contact Rab11A vesicles. In dividing cells, codistributed GFP-FIP3 and Rab11A on vesicles were observed close to the intercellular cytoplasmic bridge formed between daughter cells during cytokinesis (Figure 8Ab), supporting targeted delivery of recycling endosomal Rab11 vesicles mediated by FIP3 to the midbody (Wallace *et al.*, 2002; Horgan *et al.*, 2004; Fielding *et al.*, 2005; Wilson *et al.*, 2005). Upon infection, the ERC, costained for GFP-FIP3 and Rab11A, was delocalized to the PV (Figure 8Ba). As illustrated in orthogonal views of *z*-slices, intra-PV vesicles marked for both FIP3 and Rab11A (Figure 8Bb) or for only FIP3 or Rab11A were detected in close proximity (Figure 8Bc) or distant (Figure 8Bd) to each other. Of 60 fluorescent foci analyzed from 14 PV, 27% of the foci were yellow (positive for both FIP3 and Rab11A), 50% red (Rab11A only), and 23% GFP-labeled (FIP3 only). Although our assays could not take into account the presence of endogenous FIP3 associated with intra-PV vesicles, the detection of vesicles with GFP-FIP3 (excluding endogenous Rab11A) suggests the heterogeneous composition of host recycling vesicles sequestered into the PV.

Loss of Rab11A causes a significant decrease in the number of FIP5 but not FIP3 vesicles within the PV

Our findings suggest that mammalian vesicles with class I FIP require Rab11 binding for internalization into the PV while vesicles with class II FIP enter the PV regardless of Rab11 binding (Figures 5 and 6). To verify these observations, we silenced Rab11A expression in HeLa cells and monitored the intra-PV distribution of vesicles with endogenously expressed class I FIP5 and class II FIP3. Expression levels of Rab11A were reduced by ~90% at 2 d postdelivery of Rab11A small interfering RNA (siRNA) to HeLa cells, as measured by IFA (Figure 9, a and b). Silenced HeLa cells (Rab11A and control siRNA) were infected 2 d post–siRNA treatment before immunostaining 24 h postinfection for endogenous FIP5 or FIP3. Enumeration of PV containing endogenous FIP5 vesicles revealed 67% FIP5-positive PV (Figure 9Ba), slightly higher than the 52% of PV measured in HeLa cells expressing exogenous GFP-FIP5 (Figure 3C). The average numbers of intra-PV endogenous FIP5 (Figure 9Bb) and GFP-FIP5 (Figure 6B) vesicles were similar in both conditions, close to three. Upon Rab11A depletion, only 7% of PV contained FIP5 foci, with an average of 1.5 foci per PV. For FIP3, 88% of PV contained

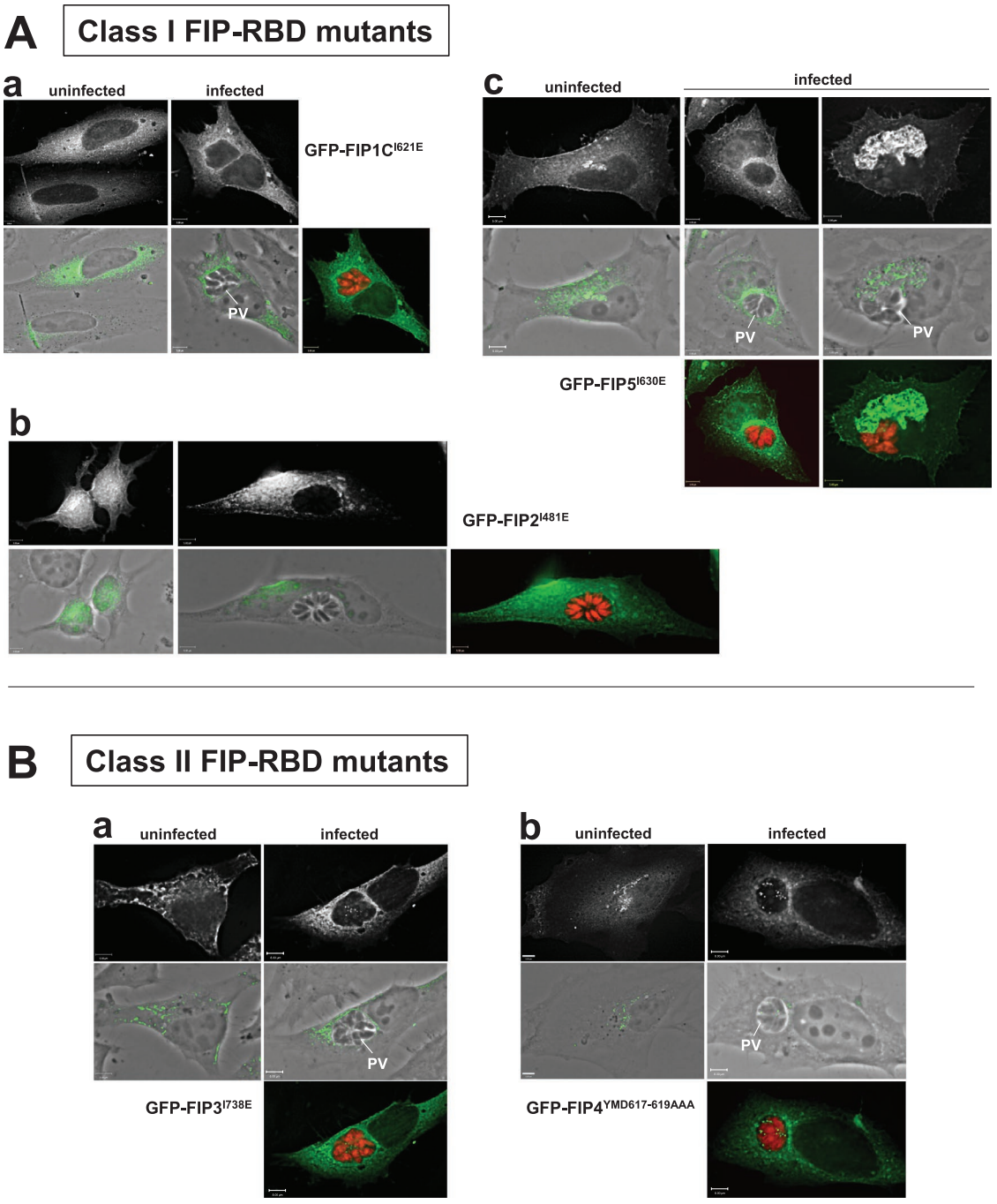

FIGURE 4: Distribution of mammalian vesicles containing FIP-RBD mutants from classes I and II in *Toxoplasma*-infected cells. (A, B) Fluorescence microscopy of HeLa cells transfected with FIP-RBD (class I in A: GFP-FIP1C^{I621E}, GFP-FIP2^{I481E}, or GFP-FIP5^{I630E}; class II in B: GFP-FIP3^{I738E} or GFP-FIP4$^{YMD617-619AAA}$) uninfected or infected with RFP-Tg for 24 h. Phase contrast overlaid with the GFP-FIP signal is shown as well as the GFP-FIP alone and with the RFP signal.

endogenous FIP3 foci, with an average of four foci per PV (Figure 9B, c and d), values comparable to PV with exogenously expressed GFP-FIP3 (Figures 3C and 6B). Depleting Rab11A in cells did not result in any significant differences in the percent of PV containing FIP3 foci or the number of FIP3 foci per PV. These data confirm the dependence of class I FIP vesicle (at least as shown for FIP5) internalization on binding to Rab11A. In contrast, despite the intra-PV detection of 27% of vesicles with Rab11A-FIP3 complexes (Figure 8), abolishing Rab11A expression in infected cells has no impact on FIP3 vesicle internalization into the PV.

Mammalian FIP3 vesicles are internalized in the PV in association with Arf6

The Rab11A-independent sequestration of FIP3 and FIP4 vesicles into the PV prompted us to investigate whether other FIP interactors were associated with class II FIP vesicles in the PV lumen. Both FIP3 and FIP4 are Arf6 effectors (Shin *et al.*, 2001). In mammalian cells, Arf6 localizes to the plasma membrane and endosomal compartments and is involved in the targeted delivery of recycling endosomal vesicles to the plasma membrane (D'Souza-Schorey and Chavrier, 2006). In preparation for cell division, Arf6 plays a vital role

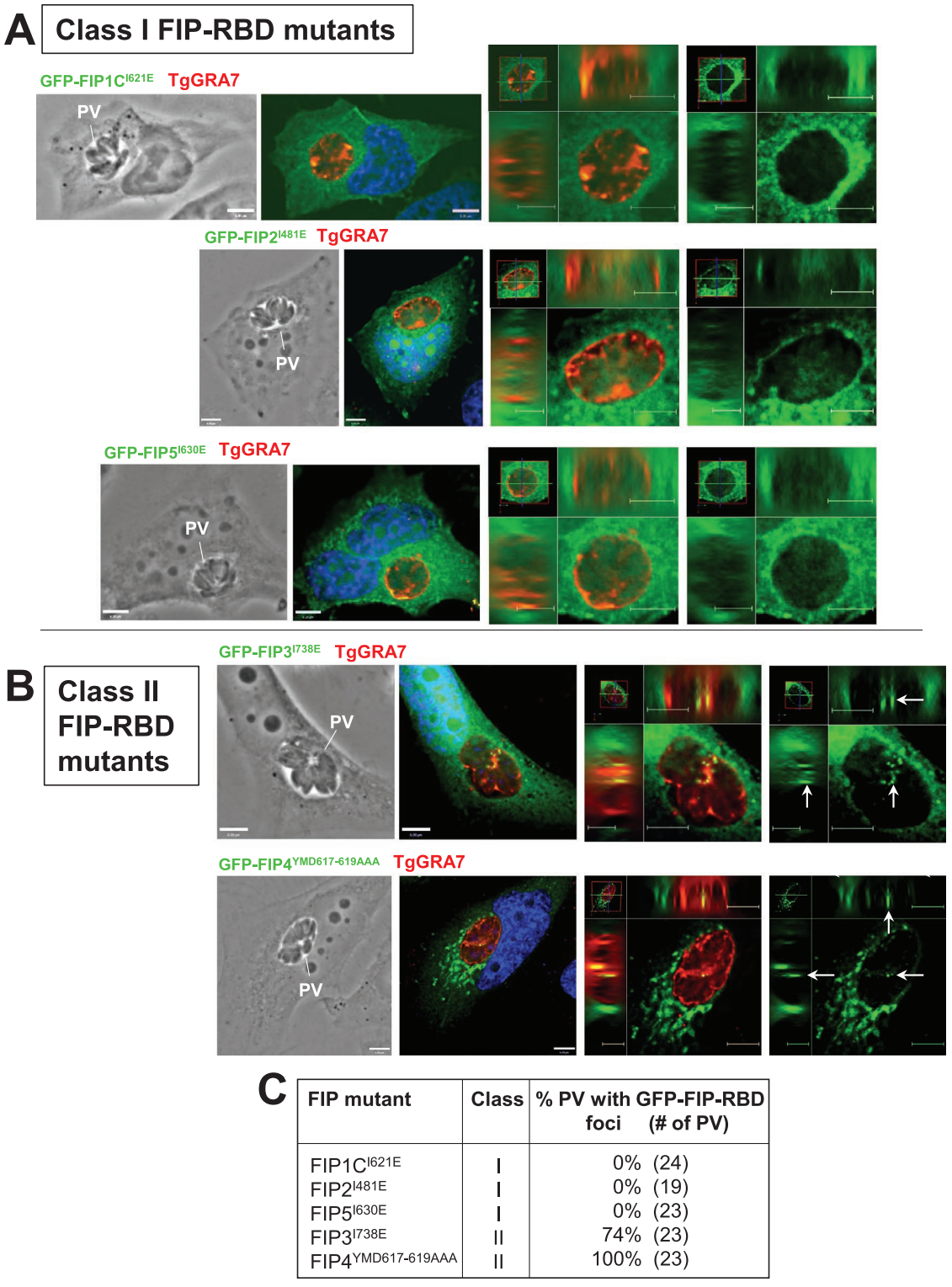

C

FIP mutant	Class	% PV with GFP-FIP-RBD foci (# of PV)
FIP1C^{I621E}	I	0% (24)
FIP2^{I481E}	I	0% (19)
FIP5^{I630E}	I	0% (23)
FIP3^{I738E}	II	74% (23)
FIP4$^{YMD617-619AAA}$	II	100% (23)

FIGURE 5: Distribution of mammalian vesicles containing FIP-RBD mutants from classes I and II in the *Toxoplasma* PV. (A, B) Fluorescence microscopy of HeLa cells transfected with FIP-RBD mutants (class I in A: GFP-FIP1C^{I621E}, GFP-FIP2^{I481E}, or GFP-FIP5^{I630E}; class II in B: GFP-FIP3^{I738E} or GFP-FIP4$^{YMD617-619AAA}$) uninfected or infected with RFP-Tg for 24 h before immunostaining with anti-TgGRA7 antibody. DAPI in blue. For all images, individual *z*-slices and orthogonal views are shown. Arrows show intra-PV GFP-FIP foci. (C) Quantification of the internalization of class I and II FIP-RBD mutant vesicles within the *Toxoplasma* PV. The percent of PV with intra-PV foci was assessed based on PV viewed in A and B.

in targeting RE, for example, Rab11 to the cleavage furrow and midbody (Schweitzer and D'Souza-Schorey, 2002). To compare the distributions of Arf6 in uninfected and *Toxoplasma*-infected cells, HeLa cells were transiently transfected with a plasmid containing Arf6 in fusion with C-terminal mCherry. In uninfected cells, the Arf6-mCherry signal was distributed in cytoplasmic structures with a

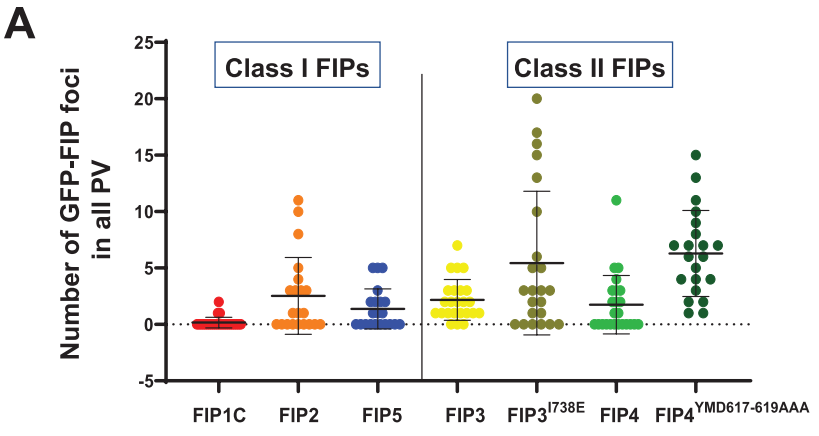

	FIP1c	FIP2	FIP3	FIP3^{I738E}	FIP4	FIP4$^{YMD617-619AAA}$
FIPC1						
FIP2	0.0048					
FIP3	0.00002	ns				
FIP3^{I738E}	0.0006	ns	0.026			
FIP4	0.0068	ns	ns	0.015		
FIP4$^{YMD617-619AAA}$	0.0000004	0.0017	0.0001	ns	0.00005	
FIP5	0.0056	ns	ns	0.007	ns	0.00001

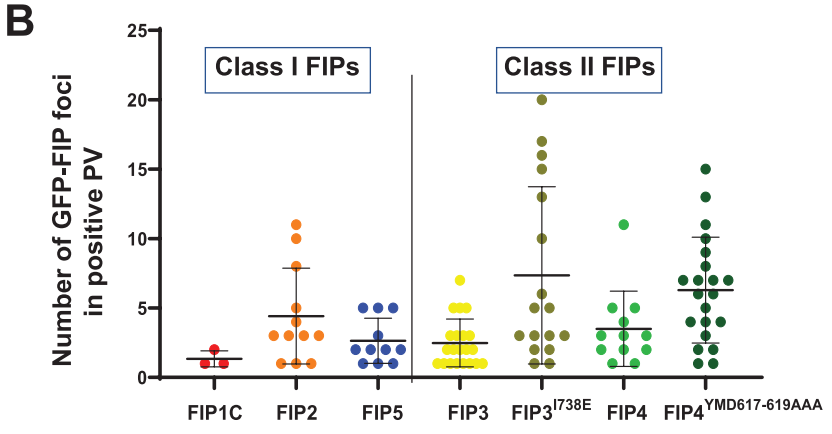

	FIP1c	FIP2	FIP3	FIP3^{I738E}	FIP4	FIP4$^{YMD617-619AAA}$
FIPC1						
FIP2	ns					
FIP3	0.05	ns				
FIP3^{I738E}	0.0014	ns	0.0068			
FIP4	0.024	ns	ns	0.036		
FIP4$^{YMD617-619AAA}$	0.00002	ns	0.0003	ns	0.02	
FIP5	0.05	ns	ns	0.009	ns	0.0007

FIGURE 6: Enumeration of Rab11-FIP or FIP-RBD mutant vesicles within the *Toxoplasma* PV. Intra-PV vesicles containing FIP or FIP-RBD mutants from classes I and II were counted based on GFP foci in all the PV (A) or only in GFP-positive PV (B). Dot plots graphs with two-tailed *p* values shown. ns, $p > 0.05$.

higher concentration at the perinuclear region (Figure 10A). When transfected cells were infected for 24 h, a strong perivacuolar staining was observed for Arf6-mCherry, suggesting interaction of the *Toxoplasma* PV with Arf6-positive vesicles (Figure 10B, a and b). Several Arf6-mCherry foci were observed within the PV, often concentrated at the IVN (Figure 10Bb).

To examine whether the parasite recognizes vesicles with both Arf6 and FIP3, we transiently transfected HeLa cells with two plasmids, one encoding GFP-FIP3 and the other Arf6-mCherry. Previous studies reported that exogenously coexpressing FIP3 and Arf6 results in increased colocalization of the two proteins (Horgan *et al.*, 2004; Fielding *et al.*, 2005). In dually transfected cells, we confirmed an intense colabeling of pericentrosomal ERC with GFP-FIP3 and Arf6-mCherry (Figure 10Ca). In dividing cells, the comigration of vesicles positive for FIP3 and Arf6 was observed at the intersection between the two daughter cells, as illustrated in panel b in Figure 10C showing midbody remnants at the cell surface after abscission. In infected cotransfected cells, the Arf6-mCherry and GFP-FIP3 signals largely overlapped at the ERC close to the PV membrane and vesicles with Arf6 and FIP3 were observed within the PV (Figure 10D). In two independent assays, 86% and 61% of PV contained Arf6-mCherry vesicles upon monotransfection or double transfection, respectively (Figure 11A). Approximately 70% of the Arf6-mCherry foci colocalized with the GFP-FIP3 foci were positive for Arf6-mCherry in cells expressing both Arf6 and FIP3. To determine whether Arf6 binding to FIP3 facilitates the Rab11-independent entry of class II FIP vesicles into the PV, we cotransfected HeLa cells with plasmids encoding Arf6-mCherry and the GFP-FIP3-RBD mutant. The Arf6-mCherry and GFP-FIP3-RBD signals were dispersed in uninfected and infected cells, with partial colocalization (Figure 11B). The perivacuolar staining for Arf6-mCherry and GFP-FIP3-RBD was weaker in dually transfected and infected cells (Figure 11B) than for infected HeLa cells transfected with Arf6-mCherry alone (Figure 9B), GFP-FIP3 alone (Figure 2Ba), or Arf6-mCherry and GFP-FIP3 (Figure 10D). In these two independent assays, only ~23% of PV contained Arf6-mCherry foci, and less than 30% of the Arf6-mCherry foci colocalized with the GFP-FIP3-RBD foci. There were also significantly fewer Arf6-mCherry foci per PV when cotransfected with GFP-FIP3-RBD as compared with cotransfection with GFP-FIP3 (Figure 12A). In comparison to the number of

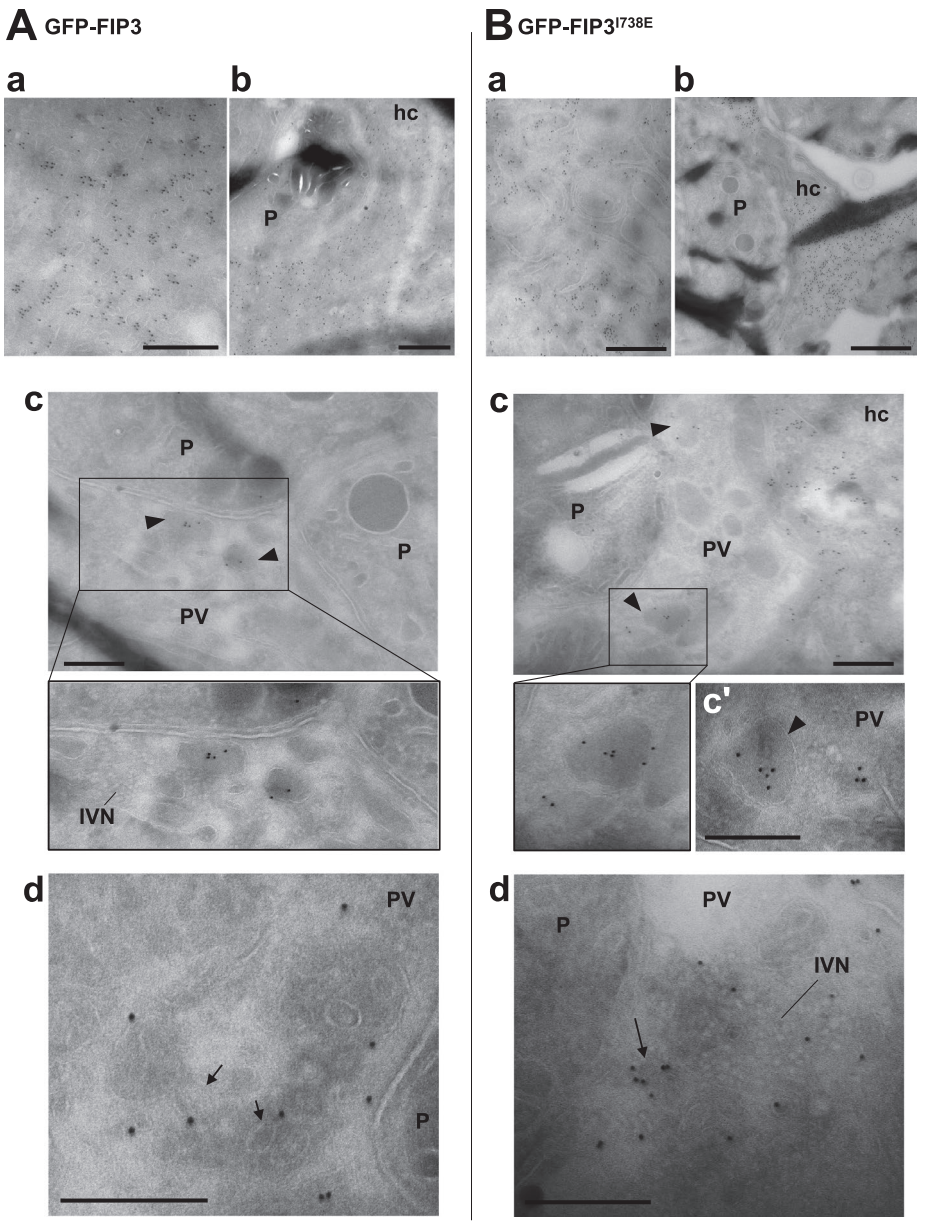

FIGURE 7: Immunolocalization of FIP3 and FIP3-RBD mutant in *Toxoplasma*-infected cells. (A, B) Immunoelectron microscopy of HeLa cells expressing GFP-FIP3 (A) or GFP-FIP3^{I738E} (B) infected for 16 h. FIP3 distribution was examined using anti-GFP antibody followed by protein A-gold particles. Panels a in A and B show gold particles in mammalian cells. Panels c, c′, and d in A and B illustrate gold particles localized within the PV on vesicles (arrowheads) and sometimes in the vicinity of the IVN. Some gold particles were also detected on the limiting membrane on internal vesicles (arrows). hc, host cell; P, parasite. All bars, 300 nm.

Arf6-mCherry foci per PV, the numbers of GFP-FIP3 or GFP-FIP3-RBD foci per PV remained constant upon double transfection (Figure 12B).

These data suggest that the presence of Rab11 complexed to FIP3 leads to more efficient internalization of Arf6 vesicles into the PV and that Arf6-FIP3 interactions may not be the driving force for the delivery of vesicles of class II FIP-RBD mutants to the PV.

Abrogation of both Rab11 and Arf6 binding to FIP3 leads to a decrease in intra-PV vesicles displaying FIP3

FIP3 binds to the C-terminal α-helix of Arf6 (Schonteich *et al.*, 2007). We generated a GFP-FIP3 construct with an altered ABD through the truncation of residues 687712 to investigate the relevance of FIP3 complexed to Arf6 for the recognition and internalization of vesicles into the PV. HeLa cells were transfected with a plasmid encoding GFP-FIP3-ABD (FIP3$^{\Delta 687\text{-}712}$) or a plasmid encoding the dual mutant GFP-FIP3-RBD-ABD (FIP3$^{I738E\Delta 687\text{-}712}$), infected, and analyzed by fluorescence microscopy. Numerous foci for GFP-FIP3-ABD vesicles were observed in the PV interior (Figure 13A) while no GFP-FIP3-RBD-ABD vesicles were detected in the vast majority of PV (Figure 13Ba). For PV in which GFP-FIP3-RBD-ABD foci were observable, the GFP signal was very weak and the foci were tiny (Figure 13Bb). The percentages of PV containing vesicles with GFP-FIP3-ABD and the numbers of these vesicles per PV (Figure 13Ca–c) were comparable to the percentage of PV with vesicles for GFP-FIP3 WT or GFP-FIP3-RBD vesicles and the intra-PV number of these vesicles (Figures 3C, 5C and 6). For the dual mutant GFP-FIP3-RBD-ABD, however, only 37% of PV were positive and the intra-PV foci were very tiny, barely detectable.

These data suggest that Rab11-FIP3 and Arf6-FIP3 interactions may not be individually required to drive FIP3 vesicle sequestration into the PV but abrogating the binding of both Rab11 and Arf6 to FIP3 is detrimental for this process. A graphical summary of our data presented in Figure 14 illustrates the class I FIP dependence on Rab11 binding for internalization and the PV's ability to internalize FIP3 vesicles depending on whether their interaction is with Rab11, Arf6, or neither.

DISCUSSION

We previously reported that the intravacuolar parasite *Toxoplasma* intercepts many host cell trafficking pathways through the sequestration of Rab vesicles into the PV (Romano *et al.*, 2013, 2017). Among them, host Rab11A and Rab11B vesicles are predominantly targeted by the parasite. The aim of this study was to examine whether *Toxoplasma* subverts distinct Rab11 subpopulations, which would suggest the parasite's ability to recognize specific Rab11 effectors or Rab11-protein complexes at the surface of vesicles before scavenging into the PV. Our in vitro assays point to a differential intra-PV internalization of host Rab11 vesicle subsets based on effector composition. These findings suggest that the PV membrane likely contains *Toxoplasma* proteins selectively involved in host Rab vesicle-PV interaction and if essential, these proteins represent potential drug targets. From a cell biological perspective, the identification of mammalian Rab effectors that are engaged in the transport of host vesicles toward the PV and intravacuolar trapping would expand our repertoire of mammalian Rab-interacting proteins.

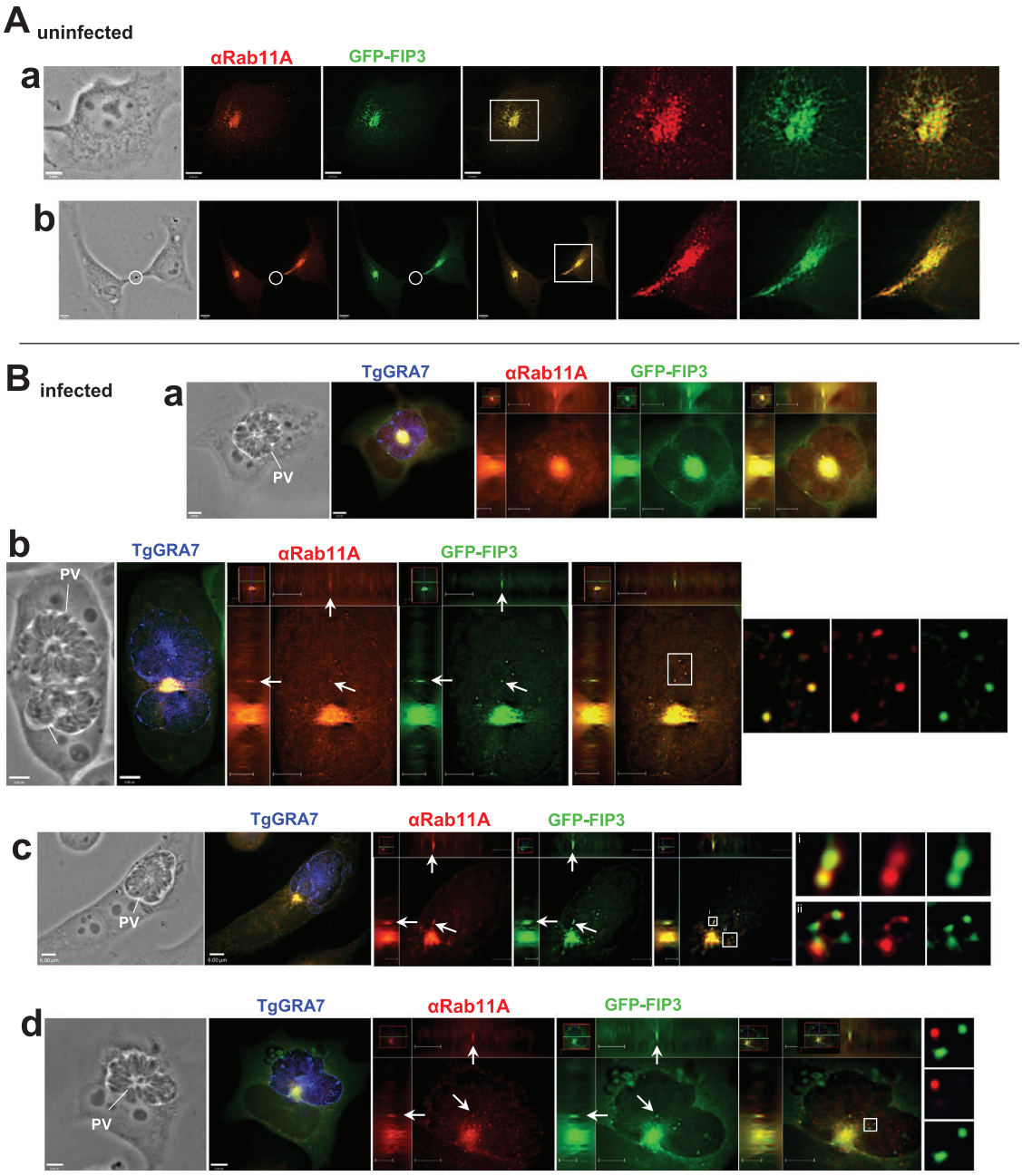

FIGURE 8: Abundance of mammalian Rab11A vesicles containing FIP3 in the PV. (A) Fluorescence microscopy of HeLa cells transfected with GFP-FIP3 and immunostained with anti-Rab11A antibody at interphase (panel a) and during cytokinesis (panel b). The circle highlights the midbody. (B) Fluorescence microscopy of HeLa cells transfected with GFP-FIP3 and infected for 24 h before immunostaining for Rab11A and TgGRA7. The delocalization of the ERC at the top of the PV or squeezed between two PV is highlighted in panels a and b, respectively. For all images, individual *z*-slices and orthogonal views are shown. Arrows and squares in panels b–d show intra-PV GFP-FIP3 foci and/or Rab11A foci.

A recent proximity-labeling study on *Toxoplasma*-infected fibroblasts aiming at identifying host proteins at the PV membrane detected FIP3 (O75154-3; Isoform 3 of Rab11 family-interacting protein 3) out of 50 human proteins putatively enriched at this membrane interface (Cygan *et al.*, 2021). This finding corroborates our morphological observations of the close proximity of FIP3 vesicles to the PV. FIP3 and FIP4 have an interacting domain for TSG101 (Horgan *et al.*, 2012), an ESCRT-I component involved in the biogenesis of the multivesicular body (Henne *et al.*, 2011). Interestingly, *Toxoplasma* secretes a dense granule protein TgGRA14 that localizes to the IVN and PV membrane, with its C-terminus exposed to the host cytosol and containing a PTAP motif for putative binding to TSG101 (Rome *et al.*, 2008). A recent study shows that mammalian TSG101 is recruited at the *Toxoplasma* PV, a process that is impaired in TgGRA14-deficient parasites (Rivera-Cuevas *et al.*, 2021). This raises the possibility that by interacting with TSG101, TgGRA14 may indirectly mediate the retention of FIP3/FIP4 vesicles at the PV membrane.

Why may Toxoplasma divert host class I FIP vesicles? Class I FIPs function in endosomal recycling processes (reviewed in Jing and Prekeris, 2009) and bind to Rab11 to govern the trafficking of Rab11 vesicles to the cell surface. *Toxoplasma* may advantageously

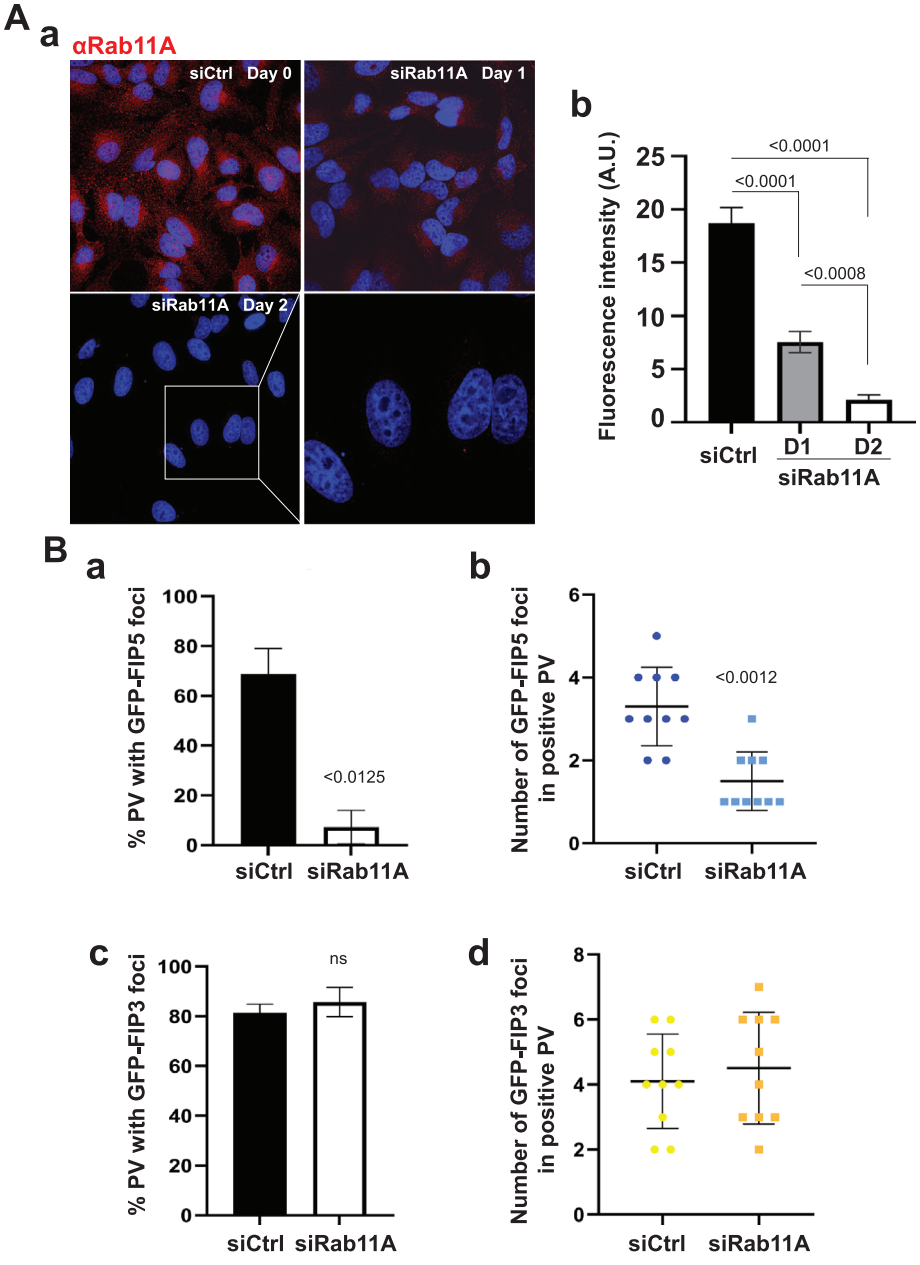

FIGURE 9: Effect of Rab11A expression on intra-PV sequestration of mammalian vesicles containing FIP5 or FIP3. (A) HeLa cells were exposed to siRNA control (day 0) or siRNA Rab11A for 1 or 2 d before IFA with anti-Rab11A antibody, showing decreased fluorescent signal (panel a). Quantification of endogenous Rab11A fluorescence levels before and after siRNA Rab11A silencing. Data and means of three independent biological samples made in triplicate. (B) Quantification of the internalization of FIP5 or FIP3 vesicles within the *Toxoplasma* PV. Panels a and c show percent of PV with at least one intra-PV focus, and panels b and d are dot plots with numbers of FIP5 or FIP3 foci per PV (two-tailed *p* values shown).

intercept class I FIP vesicles to scavenge their cargo for nutritional benefit and/or to neutralize toxic host factors through their sequestration into the PV. Among specific cargo trafficked to the cell surface by class I FIP, the glucose transporter GLUT4 is trafficked to the cell surface via FIP5 (Welsh *et al.*, 2007). FIP1C mediates the recycling of several plasma membrane receptors, including transferrin receptors (TfR), and FIP2 is implicated in the recycling of many molecules, for example, GLUT4, TfR, the water channel protein aquaporin-2, and the chemokine receptor CXCR2 (Horgan and McCaffrey, 2009).

The cargo of class I FIP vesicles may supply nutrients for replicating *Toxoplasma*. For example, the source of iron for *Toxoplasma* is still unknown, and FIP1 and FIP2 vesicles associated with TfR-Tf may provide iron to the parasite. GLUT4 is the main glucose transporter in skeletal muscle cells and fat cells, and it localizes at the plasma membrane and sorting endosomes, RE and the TGN (Bryant *et al.*, 2002). The tropism and attraction of *Toxoplasma* for skeletal muscle cells for encystation (Swierzy and Lüder, 2015) may be linked to the metabolic properties of skeletal muscle cells, such as a high glucose supply, which represent a propitious environment for the long-term survival of the parasitic chronic stage.

Toxoplasma may also target class I FIP vesicles to modulate the immune response of its host. For example, the chemokine receptor CXCR2 is present in Rab11A-positive RE (Fan *et al.*, 2003), and its recycling and thus receptor-mediated chemotaxis is regulated by FIP2 (Fan *et al.*, 2004). CXCR2 stimulates cell migration in response to a concentration gradient of the CXC chemokine IL-8 ligand (Wolf *et al.*, 1998) and is essential for the recruitment of leukocytes to inflammatory sites (Garcia-Ramallo *et al.*, 2002). Neutrophils employing a battery of microbicidal activities, for example, phagocytosis, neutrophil extracellular trap (NET) formation, and release of peroxide species, are required for early resistance against *Toxoplasma* in the gut (Sayles and Johnson, 1997; Bliss *et al.*, 2001). In particular, CXCR2 is involved in early neutrophil recruitment and plays an important protective role in resistance to *Toxoplasma* (Del Rio *et al.*, 2001). In fact, *Toxoplasma* infection of CXCR2$^{-/-}$ mice results in defects in neutrophil migration to the site of infection, lower production of proinflammatory cytokines (e.g., TNF-α, interferon gamma [IFN-γ]), and higher brain cyst numbers during chronic infection, compared with WT mice. To this point, the sequestration of vesicles containing CXCR2-FIP2 complexes into the PV may be advantageous for the parasite to avoid neutrophil attraction to infected tissues, thus ensuring parasite dissemination in the host.

In addition to CXCR2, the cargoes of Rab11 vesicles include immune mediators (Kelly *et al.*, 2012): TNF-α, which triggers IFN-γ–primed macrophages for *Toxoplasma* killing (Sibley *et al.*, 1991); IL-6, which protects during *Toxoplasma* early infection by promoting IL-17 production from NK cells for T-cell activation (Jebbari *et al.*, 1998; Passos *et al.*, 2010), and TLR4, which is a critical innate immune cell receptor involved in *Toxoplasma* detection and activation of immune responses (Zare-Bidaki *et al.*, 2014). Diversion of these anti-*Toxoplasma* effectors to the PV could be part of a strategy crafted by the parasite to thwart host cell–intrinsic innate immunity pathways.

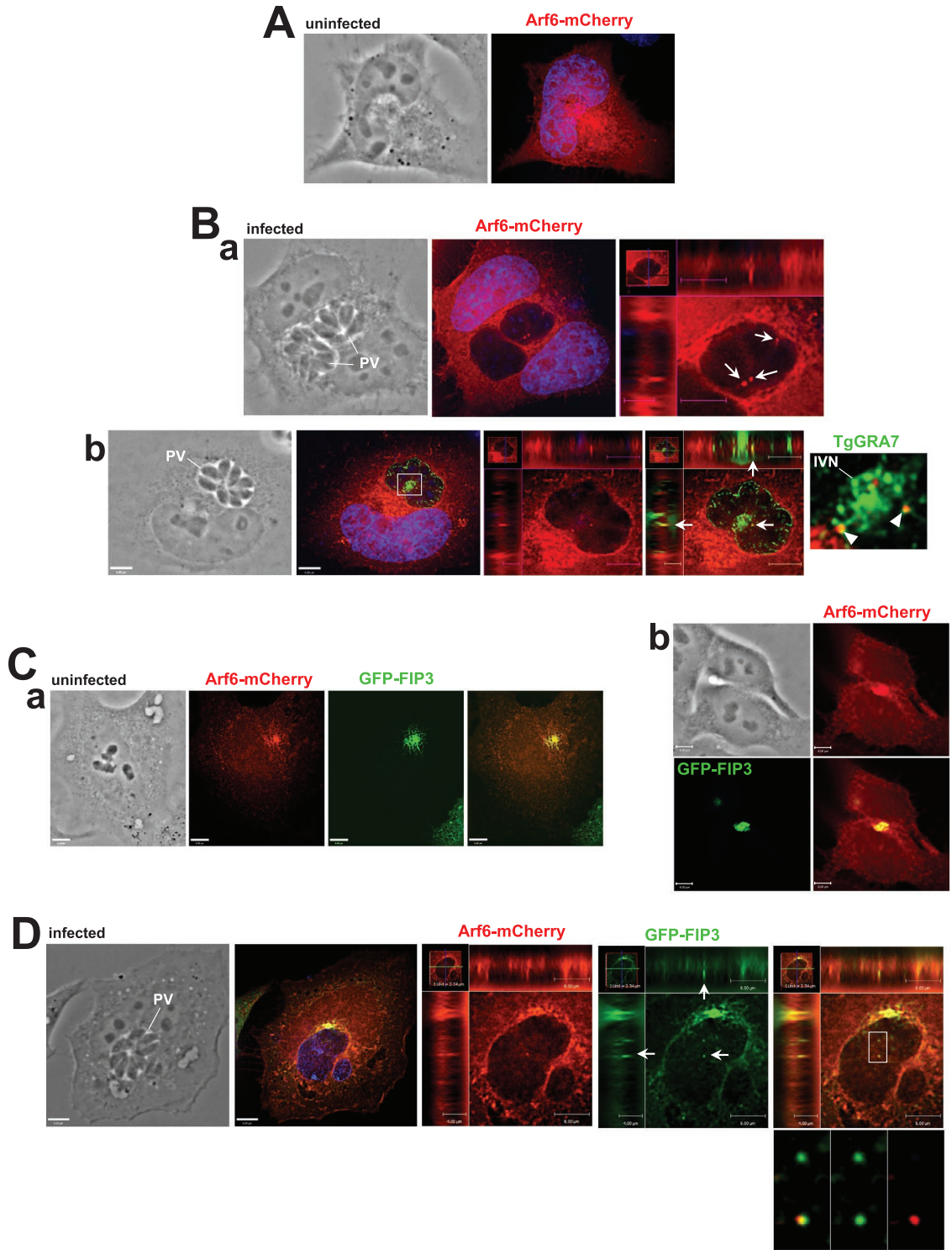

FIGURE 10: Distribution of mammalian vesicles containing Arf6 or FIP3 in *Toxoplasma*-infected cells. (A, B) Fluorescence microscopy of HeLa cells transfected with Arf6-mCherry uninfected (A) or infected for 24 h (B) before immunostaining with anti-TgGRA7 antibody (panel b). For all images, individual *z*-slices and orthogonal views are shown. Arrows show intra-PV Arf6-mCherry foci (panel a), and arrowheads pinpoint foci associated with the IVN (panel b). (C, D) Fluorescence microscopy of HeLa cells cotransfected with Arf6-mCherry and GFP-FIP3 uninfected (C, panel a: at interphase; panel b: end of cytokinesis) or infected for 24 h (D). Arrows and squares show intra-PV Arf6-mCherry and/or GFP-FIP3 foci.

The internalization of class I FIP vesicles is Rab11 dependent, suggesting the recognition of complexes formed between FIP1, FIP2, or FIP5 and Rab11. This would ensure an elective and efficient targeting of Class I FIP-Rab11 RE by the parasite to benefit from their cargoes.

Why may Toxoplasma divert host class II FIP vesicles? While class I FIP are specifically implicated in the regulation of endocytic protein sorting and recycling, class II FIP have different roles and more specialized functions depending on the cell cycle (reviewed in

A

	%PV positive with Arf6 foci (PV #)	%PV positive with FIP3/FIP3^{I738E} foci (PV #)	%Arf6 foci colocalized with FIP3/FIP3^{I738E} foci (foci #)
Arf6	86% (29)	–	–
FIP3	–	88% (24)	–
FIP3^{I738E}	–	74% (23)	–
Exp. 1 **Arf6+FIP3**	61% (23)	70% (23)	80% (54)
Exp. 1 **Arf6+FIP3 ^{I738E}**	25% (20)	80% (24)	29% (7)
Exp. 2 **Arf6+FIP3**	61% (23)	87% (23)	65% (77)
Exp. 2 **Arf6+FIP3 ^{I738E}**	21% (19)	68% (19)	0% (11)

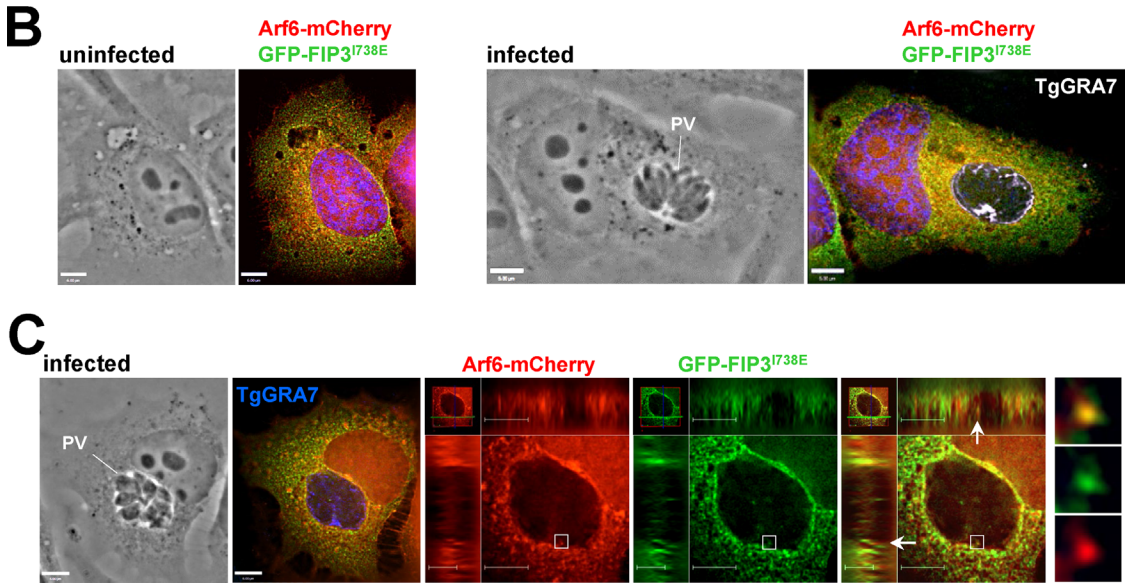

FIGURE 11: Distribution of mammalian vesicles containing Arf6 or FIP3-RBD in *Toxoplasma*-infected cells. (A) Quantitative analysis of percent of PV containing Arf6-mCherry or GFP-FIP3 and the percent of Arf6-mCherry foci that colocalized with GFP-FIP3/GFP-FIP3-RBD based on experiments described in Figure 10 and below. (B, C) Fluorescence microscopy of HeLa cells cotransfected with Arf6-mCherry and GFP-FIP3^{I738E} uninfected or infected for 24 h before immunostaining with anti-TgGRA7 antibody. For all images, individual *z*-slices and orthogonal views are shown. Arrows and squares show intra-PV GFP-FIP3-RBD foci.

Jing and Prekeris, 2009). FIP3 and FIP4 localize to the ERC and act as scaffold proteins for this organelle, tethering the ERC to the pericentrosomal region (in many cell types) through binding to microtubule motor proteins. In *Toxoplasma*-infected cells, the host ERC is dragged toward the PV. This process may be consecutive to the hijacking of the host MTOC by the parasite, resulting in the rearrangement of the host microtubular network all around the vacuole (Coppens *et al.*, 2006; Walker *et al.*, 2008). Manipulating the host microtubular network allows for the parasite to govern the host cellular membrane transport and attract organelles to the PV. Of importance, the recruitment of the host MTOC and microtubules is actively mediated by the parasite as these events also occur in mammalian cytoplasts that lack genetic materials and are, in other words, dying fragments of cytoplasm (Romano *et al.*, 2008).

The co-option of host microtubules by *Toxoplasma* is associated with supranumerous foci of γ-tubulin in infected cells, leading to host cell cycle dysregulation and defects in cytokinetic events (Molestina *et al.*, 2008; Walker *et al.*, 2008; Velasquez *et al.*, 2019). Indeed, a high proportion of infected cells exhibits chromosome segregation errors, mitotic spindle alterations, and blockage of cytokinesis progression, giving a multinucleated phenotype. At the onset of infection, *Toxoplasma* colonizes the gastrointestinal tract and replicates in intestinal epithelial cells. The self-renewal of the gut epithelium by the continuous division of cryptic stem cells is important to maintain tissue homeostasis and, in case of infection, to eliminate infected cells to thwart pathogen colonization. Thus, by counteracting host cell cytokinesis, *Toxoplasma* would delay the epithelial turnover of infected cells in the intestine and thus stabilizes its replicative niche in gut cells. During cytokinesis, FIP3 or FIP4 associated with Rab11 moves Rab11 RE to the cleavage furrow via centrosome-anchored microtubules (Fielding *et al.*, 2005). At the furrow, the Rab11-FIP3 or Rab11-FIP4 vesicles encounter and interact with Arf6 on the plasma membrane, resulting in tethering of these vesicles to the plasma membrane via interaction with the exocyst complex. In this case, the attraction and retention of FIP3, FIP4, and Arf6 vesicles in the PV may represent an additional stratagem developed by *Toxoplasma* to cause cytokinesis failure by blocking the abscission process.

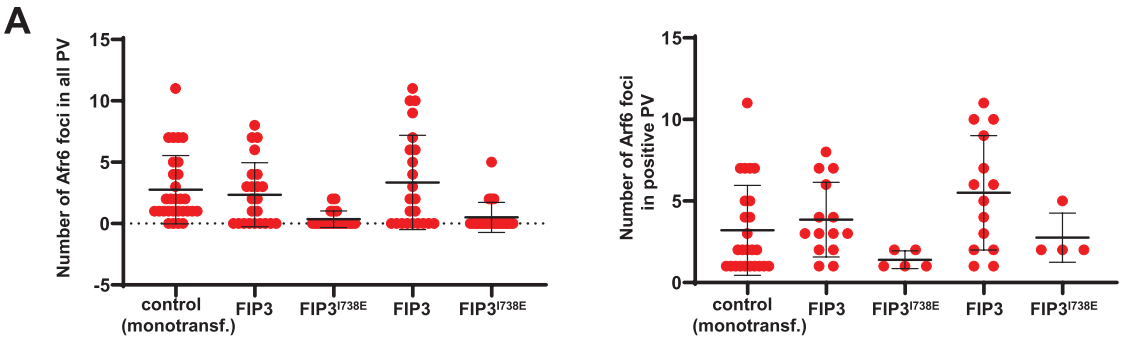

	All PV with Arf6 foci	Positive PV with Arf6 foci
Exp. 1 **Arf6+FIP3**	0.586	0.429
Exp. 1 **Arf6+FIP3^{I738E}**	0.000089	0.0058
Exp. 2 **Arf6+FIP3**	0.540	0.0457
Exp. 2 **Arf6+FIP3^{I738E}**	0.00036	0.644

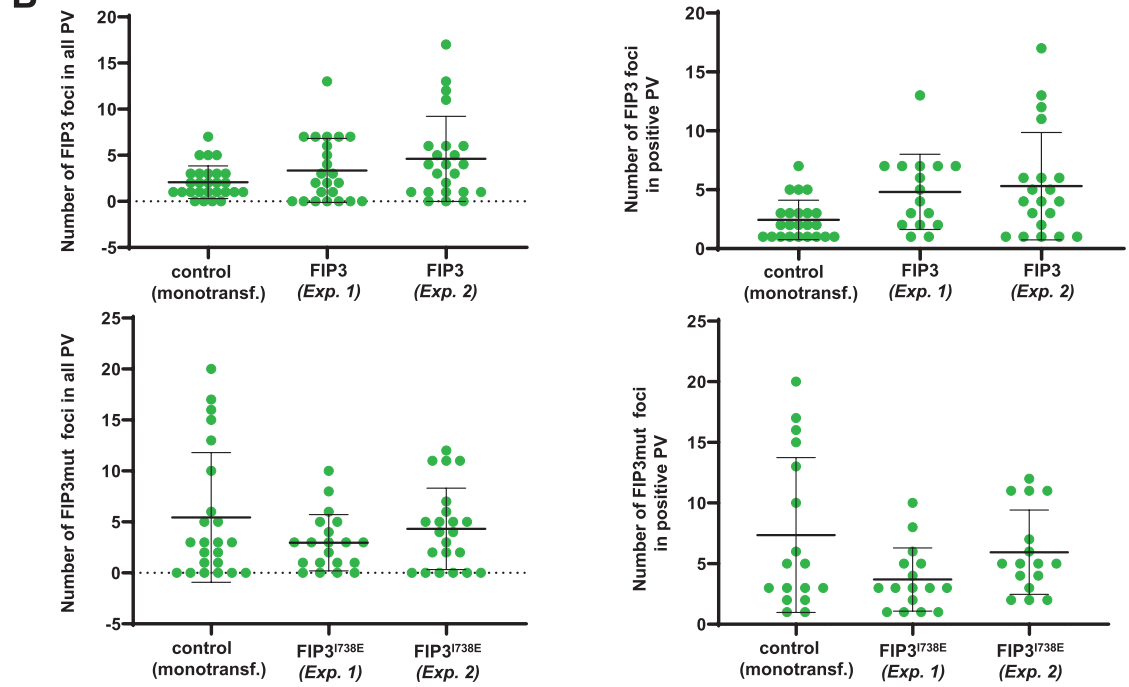

	All PV with FIP3 foci	Positive PV with FIP or FIP3^{I738E} foci
Exp. 1 **FIP3**	0.156	0.0147
Exp. 2 **FIP3^{I738E}**	0.0997	0.0403
Exp. 2 **FIP3**	0.0248	0.0156
Exp. 2 **FIP3^{I738E}**	0.483	0.433

FIGURE 12: Enumeration of foci with Arf6, FIP3, or FIP3-RBD vesicles within the *Toxoplasma* PV. (A, B) Quantification of data described in Figures 10 and 11. Intra-PV vesicles were counted in all the PV or all the positive PV for Arf6-mCherry (in A) or GFP-FIP3/GFP-FIP3-RBD (in B). Dot plots and tables show two-tailed *p* values compared with control conditions corresponding to monotransfected HeLa cells with Arf6-mCherry, GFP-FIP3, or GFP-FIP3$^{\Delta 687\text{-}712}$.

Alternatively, the primary target of *Toxoplasma* may be the host ERC, which is pulled toward the PV subsequently to MTOC capture. The ERC is a long-lived compartment, with multiple sorting functions toward the recycling, retrograde, and exocytic routes (Maxfield and McGraw, 2004). Most proteins that cycle between the cell interior and the cell surface accumulate in the ERC because this is the slow step in their return to the plasma membrane. For example, all of the LDL receptors and TfR recycle from the ERC to the cell surface.

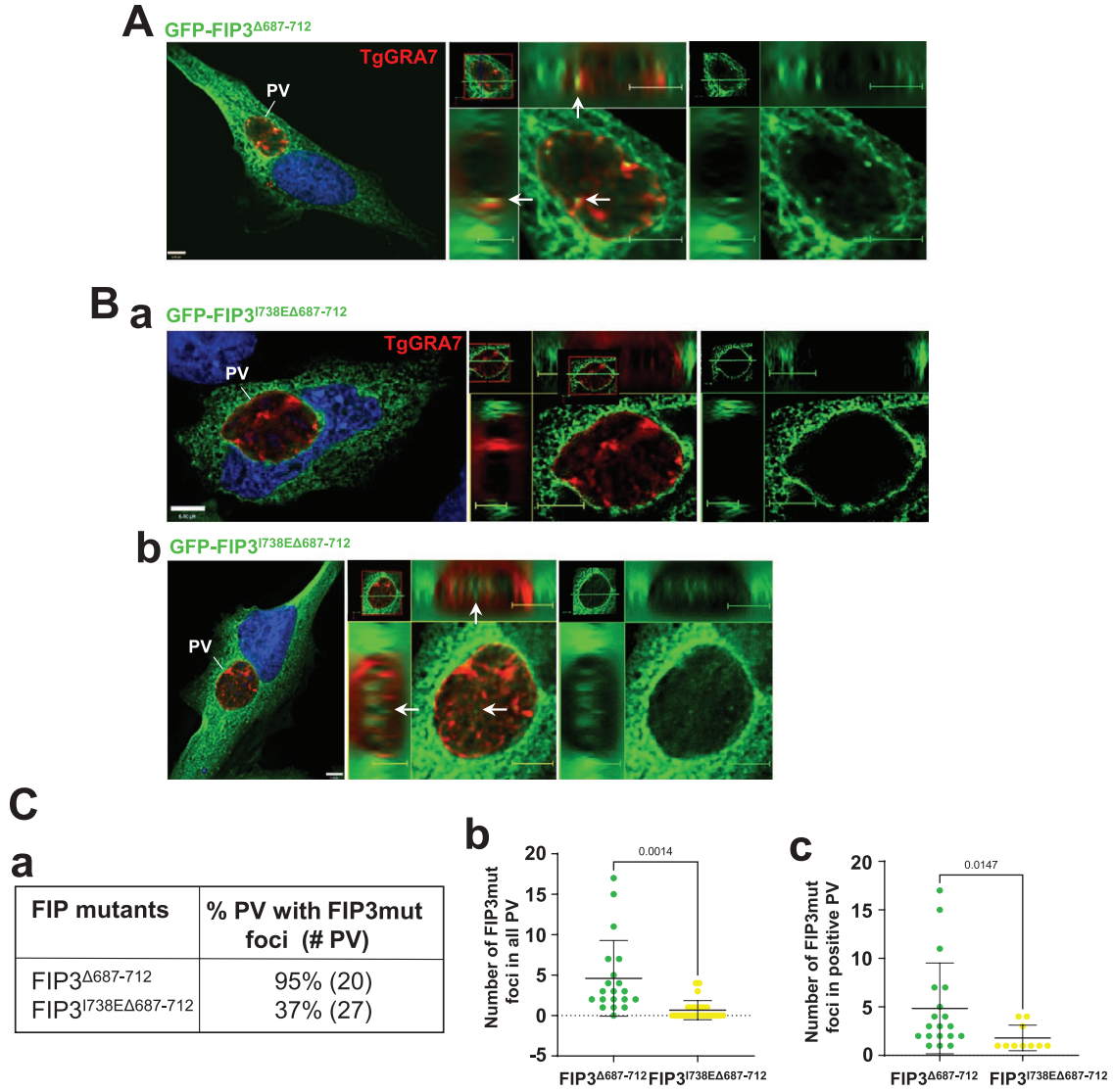

FIP mutants	% PV with FIP3mut foci (# PV)
FIP3$^{\Delta 687\text{-}712}$	95% (20)
FIP3$^{I738E\Delta 687\text{-}712}$	37% (27)

FIGURE 13: Comparative distribution of mammalian vesicles containing Rab11-FIP3-ABD and Rab11-FIP3-RBD-ABD in the *Toxoplasma* PV. (A, B) Fluorescence microscopy of HeLa cells cotransfected with GFP-FIP3$^{\Delta 687\text{-}712}$ (A) or GFP-FIP3$^{I738E\Delta 687\text{-}712}$ (B, b and c) and infected for 24 h before immunostaining with anti-TgGRA7 antibody. DAPI in blue. For all images, individual *z*-slices and orthogonal views are shown. Arrows show intra-PV foci. C. Percent of PV with intra-PV foci corresponding to vesicles with GFP-FIP3-ABD or GFP-FIP3-RBD-ABD (panel a) and enumeration of mammalian intra-PV vesicles with GFP-FIP3-ABD or GFP-FIP3-RBD-ABD mutants in all PV (panel b) or PV positive for GFP (panel c). Dot plot graphs with two-tailed *p* values are shown.

The ERC is also a major repository of cholesterol that enters the organelle by endocytosis and nonvesicular mechanisms (Hao *et al*, 2002). A prime example of essential metabolites for the parasite is cholesterol, which is derived from LDL that are internalized into the host cell (Coppens *et al*., 2000). *Toxoplasma* also relies on host sphingolipids for optimal replication (Romano *et al*., 2013), and sphingomyelin transits through the ERC before delivery to various intracellular destinations (Koval and Pagano, 1989). The ERC may then represent a source of endogenous and exogenous metabolites for *Toxoplasma*, and targeting the ERC for its massive pool of cholesterol and sphingolipids would be advantageous for the parasite.

The proximity of the ERC to the PV would also facilitate the scavenging of FIP3 and FIP4 vesicles by the parasite. The ERC is composed of both Rab11- and Arf6-positive membrane subsets. The trapping of FIP3 and FIP4 vesicles inside the PV is Rab11 independent, suggesting a mechanism of internalization for class II FIP vesicles different from class I FIP vesicles, such as the mediation of Arf6 for recognition and scavenging of class II FIP vesicles. Overall, our data highlight a selective process of interaction with host vesicular components at the PV membrane, likely mediated by specific parasite proteins.

Arf6 mediates a clathrin-independent endocytosis (CIE) pathway, in which cargo is internalized and transported in Arf6-enriched vesicles to be subsequently recycled to the plasma membrane (Van Acker *et al*., 2019). Thus, like Rab11-associated vesicles, Arf6-associated endosomes may play roles in nutrient acquisition or immune response control. Arf6-associated endosomes carry cholesterol, and Arf6 is a central regulator of cholesterol homeostasis, controlling both the uptake and efflux of this lipid from cells (Naslavsky *et al*., 2004; Schweitzer *et al*., 2009). Therefore, the intra-PV Arf6 vesicles may constitute a providential source of cholesterol for *Toxoplasma*. Additional potential nutrient modulating cargo for Arf6-associated

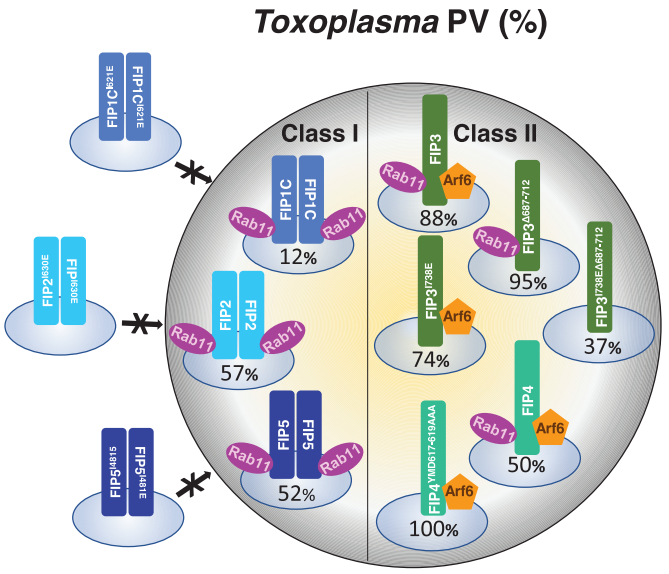

FIGURE 14: Graphical summary of the differential internalization of mammalian FIP recycling vesicles into the *Toxoplasma* PV. The percentage of positive PV containing FIP-associated vesicles is shown. The percentage of PV containing recycling vesicles marked with a WT or RBD-mutant FIP from class I or class II is indicated, revealing selectivity for PV internalization among FIP vesicles. No vesicles with class I FIP-RBD mutants are detected in the PV, while vesicles with class II FIP-RBD mutants are still internalized with PV containing vesicles with FIP4-RBD. Vesicles with FIP3-RBD or FIP3-ABD are internalized into PV. Very few PV display vesicles with the dual mutant FIP3-RBD-ABD.

endosomes include the glucose transporter GLUT1 and some amino acid transporters. MHC class I molecules are also present on Arf6-positive tubules emanating from the ERC. It has been reported that cross presentation by MHC class I molecules, which allow the detection of exogenous antigens by $CD8^+$ T-lymphocytes, is crucial to initiate cytotoxic immune responses against *Toxoplasma* (Blanchard *et al.*, 2008). Interestingly, the Δgra2Δgra6 *Toxoplasma* mutant that lacks the IVN and is impaired in intra-PV vesicle internalization is more susceptible to MHC I presentation than WT parasites (Lopez *et al.*, 2015). This suggests that the scavenging of Arf6 vesicles could be an immune regulatory process mediated by the parasite to interfere with antigen cross presentation and immune detection.

MATERIALS AND METHODS

Request a protocol through *Bio-protocol*.

Reagents and antibodies

All reagents were purchased from Sigma (St. Louis, MO) or Thermo Fisher Scientific (Waltham, MA), unless otherwise stated. The primary antibodies used in this study were rat and rabbit polyclonal anti-GRA7 (Coppens *et al.*, 2006), rabbit anti-Rab11 (Cell Signaling Technologies, Danvers, MA), rabbit anti-FIP3 and anti-FIP5 (Novus Biologicals, Centennial, CO), mouse anti-NTPase (gift from J. F. Dubremetz, University of Montpellier, France), and rabbit anti-Rab11A (Cell Signaling Technologies). The anti-Rab11A antibody was selected to specifically recognize human Rab11A (excluding human Rab11B and *Toxoplasma* Rab11) based on the unique sequence at the C-terminus from amino acid 181 to amino acid 216 in human Rab11A. Secondary antibodies from Thermo Fisher Scientific included anti-rat conjugated to Alexa Fluor 350, Alexa Fluor 488, or Alexa Fluor 594 and anti-rabbit conjugated to Alexa Fluor 594 or Alexa Fluor 647.

Cell and parasite cultivation

Vero cells, HeLa cells, and human foreskin fibroblasts (HFF) were obtained from the American Type Culture Collection (Manassas, VA). Cells were maintained in αMEM with 10% (vol/vol) fetal bovine serum (FBS), 100 U/ml penicillin/streptomycin (Quality Biological, Gaithersburg, MD), and 2 mM L-glutamine (complete αMEM culture medium) at 37°C and 5% CO_2. The Vero cells stably expressing GFP-Rab11A (Romano *et al.*, 2017) were cultivated in complete culture αMEM containing 800 µg/ml G418. *Toxoplasma* tachyzoites (type 1 RH), WT and transgenic strains, were serially passaged in six-well plates on confluent monolayers of HFF by transferring the supernatant containing egressed tachyzoites from one well to another (Roos *et al.*, 1995). The RFP-expressing RH strain (RFP-Tg) was provided by F. Dzierszinski (McGill University, Montreal, Canada; Dzierszinski *et al.*, 2004). The RH strain with *gra2* and *gra6* knocked out (Δgra2Δgra6) was provided by MF Cesbron-Delauw (Université Grenoble Alpes, Grenoble, France; Mercier*et al.*, 2002).

Toxoplasma infection of mammalian cells

Transfected cells were infected 4 h following transfection, and untransfected cells were infected approximately 24–48 h after plating at 60% confluency. For infection, media was removed from the cells on coverslips in wells from a 24-well plate, and freshly egressed parasites were added for 30 min. The coverslips were then washed with prewarmed phosphate-buffered saline (PBS) to remove extracellular (noninvading) parasites allowing for synchronization of infection. The infections proceeded for 24 h to yield four to eight parasites per PV.

Plasmids

The plasmids GFP-FIP1C, GFP-FIP1C^{I621E}, GFP-FIP2, GFP-FIP2^{I480E}, GFP-FIP3, GFP-FIP3^{I738E}, GFP-FIP4, GFP-FIP4$^{YMD617\text{-}619AAA}$, GFP-FIP5, and GFP-FIP5^{I630E} were generously provided by M. McCaffrey (University College Cork, Cork, Ireland). Their sequences were verified using the standard CMV-For primer and our primer oJR81 5′ GGGAGGTGTGGGAGGTTTT 3′. The Arf6-mCherry plasmid pcDNA3/hArf6(WT)-mCherry was a gift from Kazuhisa Nakayama (Addgene plasmid # 79422; http://n2t.net/addgene:79422; RRID:Addgene_79422; Makyio *et al.*, 2012), and the sequence was confirmed using standard CMV-For and BGH-Rev primers. The plasmids containing ABD deletion mutant (GFP-FIP3-ABD) and the ABD and Rab11-binding domain (RBD) mutant (GFP-FIP3-I738E-ABD) were engineered from the McCaffrey plasmids GFP-FIP3 and GFP-FIP3^{I738E} using the Q5 Mutagenesis Kit (New England Biolabs, Ipswich, MA) following the manufacturer instructions. To generate the FIP3-ABD mutant, amino acids 687–712 were deleted using primers ABDdlt_F 5′ AGCTCCGTCTCCCGAGAT 3′ and ABDdlt_R 5′ CCCGTTCAGCTCCTCGTT 3′. The same pair of primers was used for both pEGFP-c1-FIP3 and pEGFP-c1-FIP3 2-756 I738E using an annealing temperature of 68°C with 3% dimethyl sulfoxide added to the PCR. Transformed bacteria were grown on Lauria-Bertani (LB)-agar plates containing kanamycin overnight and then cultured in 3 ml of LB with kanamycin for 22 h at 37°C at 220 rpm. After transformation and overnight culture, the Qiaprep Spin Miniprep Kit (Qiagen, Germantown, MD) was used to isolate the plasmid, and Sanger sequencing using primer oJR81 was used to confirm the sequence of the FIP3-ABD and FIP3-RBD-ABD mutant plasmids.

Mammalian cell transfection

Vero cells were transfected with 2 µg of plasmid DNA in Amaxa Nucleofector solution R (Lonza Bioscience, Rockville, MD), following the manufacturer's instructions with program V-01. Transfected Vero

cells were then plated on coverslips in 24-well plates and allowed to recover for 24 h before infection or fixation. HeLa cells were plated on coverslips in 24-well plates at the confluency of 45–50% 24–48 h before transfection using jetPrime (Polyplus-transfection, New York, NY) for 4 h following the manufacturer's instructions. Recommended DNA and reagents for HeLa cells were adjusted to 0.2 µg of plasmid DNA, 0.4 µl of jetPrime reagent, and 50 µl of jetPrime buffer per well to minimize cell toxicity.

Mammalian cell silencing for Rab11A

HeLa cells were transfected with Rab11a siRNA using jetPrime siRNA transfection reagents (Polyplus). The siRNA duplexes were purchased from Santa Cruz Biotechnology (sc-36340) and consist of a pool of three target-specific 19–25 nucleotide siRNAs designed to knock down gene expression of the human Rab11A genetic locus (chromosomal locations maps to 15q22.31). siRNA sequences of the sense strands are as follows: sc-36340A (5′-GUAGAGUUUGCAACAAGAAtt-3′), sc-36340B (5′-CCUAGACUCUACAAAUGUAtt-3′), and sc-36340C (5′-GCAUUGUAGAGAUCUGAAAtt-3′). HeLa cells were grown to 50% confluency before exposure to the siRNA pool for 24 h. Quantification of siRNA fluorescence levels for Rab11A by IFA using rabbit anti-Rab11A antibody revealed goat anti-rabbit Alexa Fluor 647 secondary antibody was performed by averaging specific fluorescence intensity across three randomly selected fields of view (FOV) with 10 HeLa cells at $t = 0$, 24, and 48 h after Rab11A siRNA exposure. A control for background fluorescence was achieved using goat anti-rabbit Alexa Fluor 647 secondary antibody alone, with fluorescence value histograms acquired from this control applied to all FOVs analyzed. Each FOV was from an independent biological replicate ($n = 3$). HeLa cells were used for *Toxoplasma* infection 48 h after siRNA exposure.

Immunofluorescence assay

Cells were fixed in a solution of 4% formaldehyde (Electron Microscopy Sciences, Hatfield, PA) and 0.02% glutaraldehyde (EMS) for 15 min at room temperature and permeabilized with 0.3% Triton X-100 for 5 min at room temperature. Cells were blocked with 3% bovine serum albumin (BSA) for 1 h at room temperature before addition of the primary antibody diluted in 3% BSA for 1 h at room temperature or overnight at 4°C. Secondary antibodies diluted in 3% FBS were added to the coverslip for 1 h incubation at room temperature. To stain nuclei, coverslips were incubated with 4′,6-diamidino-2-phenylindole (DAPI) at 1 µg/ml in water for 5 min at room temperature. Coverslips were then mounted with the Prolong Gold or Diamond antifade mounting solution.

Fixed cell imaging and analysis

Cells were imaged on a Zeiss Axioimager M2 fluorescence microscope with a z motor for acquisition of slices along the *z*-axis. An oil-immersion Zeiss plan Apo 100×/NA 1.4 objective and a Hamamatsu ORCA-R2 camera were used to acquire images with optical *z*-slices of 0.2 µm. Images were acquired, registry corrected, deconvolved, and brightness/contrast adjusted using Volocity imaging software version 6.3 or 6.3.1 (Perkin Elmer, Waltham, MA). Fluorescent foci in the PV were identified and counted manually after identifying the boundaries of the PV based on the change in fluorescence patterns of the fluorescently tagged proteins. Statistical differences were determined using unpaired, two-tailed *T* tests with the Welch's correction for unequal SDs with Prism (Graphpad, San Diego, CA). PV were ranked as positive based on one or more distinct fluorescent foci detected within the bounds of the PV or negative if no foci could be observed inside the PV.

Immunoelectron microscopy

For immunogold staining of GFP-FIP3 and GFP-FIP3-RBD, *Toxoplasma*-infected cells were fixed in 4% paraformaldehyde (Electron Microscopy Sciences) in 0.25 M HEPES (ph 7.4) for 1 h at room temperature and then in 8% paraformaldehyde in the same buffer overnight at 4°C. They were infiltrated, frozen, and sectioned as described (Romano *et al.*, 2017). The sections were immunolabeled with antibodies against GFP (Clontech Laboratories, Mountain View, CA) at 1:25 diluted in PBS/1% fish skin gelatin and then with secondary immunoglobulin G antibodies coupled to 10 nm protein A-gold particles before examination with a Philips CM120 EM (Eindhoven, the Netherlands) under 80 kV.

ACKNOWLEDGMENTS

We thank the members of the Coppens' laboratory for helpful discussion during the course of this work and especially Karen Ehrenman for her help for the cloning of the ABD mutant. We are also grateful to the generous providers of antibodies, plasmids, and parasite strains used in this study. We thank the excellent technical staff and Kim Zichichi of the Electron Microscopy Core Facility at Yale School of Medicine. This study was supported by the grant from the National Institutes of Health, AI060767, to I. C. and a predoctoral fellowship from the American Heart Association to E.J.H.

REFERENCES

Best JM, Foell JD, Buss CR, Delisle BP, Balijepalli RC, January CT, Kamp TJ (2011). Small GTPase Rab11b regulates degradation of surface membrane L-type Cav1.2 channels. Am Physiol Cell Physiol 300, C1023–C1033.

Bhuin T, Roy JK (2015). Rab11 in disease progression. Int J Mol Cell Med 4, 1–8.

Blanchard N, Gonzalez F, Schaeffer M, Joncker NT, Cheng T, Shastri AJ, Robey EA, Shastri N (2008). Immunodominant, protective response to the parasite Toxoplasma gondii requires antigen processing in the endoplasmic reticulum. Nat Immunol 9, 937–944.

Bliss SK, Gavrilescu LC, Alcaraz A, Denkers EY (2001). Neutrophil depletion during Toxoplasma gondii infection leads to impaired immunity and lethal systemic pathology. Infect Immun 69, 4898.

Bryant NJ, Govers R, James DE (2002). Regulated transport of the glucose transporter GLUT4. Nat Rev Mol Cell Biol 3, 267–277.

Butterworth MB, Edinger RS, Silvis MR, Gallo LI, Liang X, Apodaca G, Fizzell RA, Johnson JP (2012). Rab11b regulates the trafficking and recycling of the epithelial sodium channel (ENaC). Am J Physiol Renal Physiol 302, F581–F590.

Casanova JE, Wang X, Kumar R, Bhartur SG, Navarre J, Woodrum JE, Altschuler Y, Ray GS, Goldenring JR (1999). Association of Rab25 and Rab11a with the apical recycling system of polarized Madin–Darby canine kidney cells. Mol Biol Cell 10, 47–61.

Caswell PT, Chan M, Lindsay AJ, McCaffrey MW, Boettiger D, Norman JC (2008) Rab-coupling protein coordinates recycling of α5β1 integrin and EGFR1 to promote cell migration in 3D microenvironments. J Cell Biol 183, 143–155.

Chavrier P, Goud B (1999). The role of ARF and Rab GTPases in membrane transport. Curr Opin Cell Biol 11, 466–475.

Coppens I, Dunn JD, Romano JD, Pypaert M, Zhang H, Boothroyd JC, Joiner KA (2006). *Toxoplasma gondii* sequesters lysosomes from mammalian hosts in the vacuolar space. Cell 125, 261–274.

Coppens I, Romano JD (2020). Sitting in the driver's seat: manipulation of mammalian cell Rab GTPase functions by apicomplexan parasites. Biol Cell 112, 187–195.

Coppens I, Sinai AP, Joiner KA (2000). *Toxoplasma gondii* exploits host low-density lipoprotein receptor-mediated endocytosis for cholesterol acquisition. J Cell Biol 149, 167–180.

Cox D, Lee DJ, Dale BM, Calafat J, Greenberg S (2000). A Rab11-containing rapidly recycling compartment in macrophages that promotes phagocytosis. Proc Natl Acad Sci USA 97, 680–685.

Cygan AM, Beltran PMJ, Mendoza AG, Branon TC, Ting AY, Carr SA, Boothroyd JC (2021). Proximity-labeling reveals novel host and parasite proteins at the *Toxoplasma* parasitophorous vacuole membrane. mBio 12, e0026021.

Del Rio L, Bennouna S, Salinas J, Denkers EY (2001). CXCR2 deficiency confers impaired neutrophil recruitment and increased susceptibility during *Toxoplasma gondii* infection. J Immunol 167, 6503–6509.
D'Souza-Schorey C, Chavrier P (2006). ARF proteins: roles in membrane traffic and beyond. Nat Rev Mol Cell Biol 7, 347–358.
Dzierszinski F, Nishi M, Ouko L, Roos DS (2004). Dynamics of *Toxoplasma gondii* differentiation. Eukaryot Cell 3, 992–1003.
Eathiraj S, Mishra A, Prekeris R, Lambright DG (2006). Structural basis for Rab11-mediated recruitment of FIP3 to recycling endosomes. J Mol Biol 364, 121–135.
Fan GH, Lapierre LA, Goldenring JR, Richmond A (2003). Differential regulation of CXCR2 trafficking by Rab GTPases. Blood 101, 2115–2124.
Fan GH, Lapierre LA, Goldenring JR, Sai J, Richmond A (2004). Rab11-family interacting protein 2 and myosin Vb are required for CXCR2 recycling and receptor-mediated chemotaxis. Mol Biol Cell 15, 2456–2469.
Fielding AB, Schonteich E, Matheson J, Wilson G, Yu X, Hickson GR, Srivastava S, Baldwin SA, Prekeris R, Gould GW (2005). Rab11-FIP3 and FIP4 interact with Arf6 and the exocyst to control membrane traffic in cytokinesis. EMBO J 24, 3389–3399.
Garcia-Ramallo E, Marques T, Prats N, Beleta J, Kunkel SL, Godessart N (2002). Resident cell chemokine expression serves as the major mechanism for leukocyte recruitment during local inflammation. J Immunol 169, 6467–6473.
Grant BD, Donaldson JG (2009). Pathways and mechanisms of endocytic recycling. Nat Rev Mol Cell Biol 10, 597–608.
Hao M, Lin SX, Karylowski OJ, Wüstner D, McGraw TE, Maxfield FR (2002). Vesicular and non-vesicular sterol transport in living cells. The endocytic recycling compartment is a major sterol storage organelle. J Biol Chem 277, 609–617.
Hara Y, Fukaya M, Hayashi K, Kawauchi T, Nakajima K, Sakagami H (2006). ADP ribosylation factor 6 regulates neuronal migration in the developing cerebral cortex through FIP3/arfophilin-1-dependent endosomal trafficking of N-cadherin. eNeuro, ENEURO.0148-16.
Henne WM, Buchkovich NJ, Emr SD (2011). The ESCRT pathway. Dev Cell 21, 77–91.
Horgan CP, Hanscom SR, Kelly EE, McCaffrey MW (2012). Tumor susceptibility gene 101 (TSG101) is a novel binding-partner for the class II Rab11-FIPs. PLoS One 7, e32030.
Horgan CP, McCaffrey MW (2009). The dynamic Rab11-FIPs. Biochem Soc Trans 37, 1032–1036.
Horgan CP, Oleksy A, Zhdanov AV, Lall PY, White IJ, Khan AR, Futter CE, McCaffrey JG, McCaffrey MW (2007). Rab11-FIP3 is critical for the structural integrity of the endosomal recycling compartment. Traffic 8, 414–430.
Horgan CP, Walsh M, Zurawski TH, McCaffrey MW (2004). Rab11-FIP3 localises to a Rab11-positive pericentrosomal compartment during interphase and to the cleavage furrow during cytokinesis. Biochem Biophys Res Commun 319, 83–94.
Jagoe WN, Lindsay AJ, Read RJ, McCoy AJ, McCaffrey MW, Khan AR (2006). Crystal structure of Rab11 in complex with Rab11 family interacting protein 2. Structure 14, 1273–1283.
Jebbari H, Roberts CW, Ferguson DJ, Bluethmann H, Alexander J (1998). A protective role for IL-6 during early infection with *Toxoplasma gondii*. Parasite Immunol 20, 231–239.
Jing J, Prekeris R (2009). Polarized endocytic transport: the roles of Rab11 and Rab11-FIPs in regulating cell polarity. Histol Histopathol 24, 1171–1180.
Junutula JR, Schonteich E, Wilson GM, Peden AA, Scheller RH, Prekeris R (2004). Molecular characterization of Rab11 interactions with members of the family of Rab11-interacting proteins. J Biol Chem 279, 33430–33437.
Kelly EE, Horgan CP, McCaffrey MW (2012). Rab11 proteins in health and disease. Biochem Soc Trans 40, 1360–1367.
Kelly EE, Horgan CP, McCaffrey MW, Young P (2011). The role of endosomal-recycling in long-term potentiation. Cell Mol Life Sci 68, 185–194.
Khvotchev MV, Ren M, Takamori S, Jahn R, Sudhof TC (2003). Divergent functions of neuronal Rab11b in Ca^{2+}-regulated versus constitutive exocytosis. J Neurosci 23, 10531–10539.
Koval M, Pagano RE (1989). Lipid recycling between the plasma membrane and intracellular compartments: transport and metabolism of fluorescent sphingomyelin analogues in cultured fibroblasts. J Cell Biol 108, 2169–2181.
Lindsay AJ, Hendrick AG, Cantalupo G, Senic-Matuglia F, Goud B, Bucci C, McCaffrey MW (2002). Rab coupling protein (RCP), a novel Rab4 and Rab11 effector protein. J Biol Chem 277, 12190–12199.
Lindsay AJ, McCaffrey MW (2004a). Characterisation of the Rab binding properties of Rab coupling protein (RCP) by site-directed mutagenesis. FEBS Lett 571, 86–92.
Lindsay AJ, McCaffrey MW (2004b). The C2 domains of the class I Rab11 family of interacting proteins target recycling vesicles to the plasma membrane. J Cell Sci 117, 4365–4375.
Lopez J, Bittame A, Massera C, Vasseur V, Effantin G, Valat A, Buaillon C, Allart S, Fox BA, Rommereim LM, *et al*. (2015). Intravacuolar membranes regulate CD8 T cell recognition of membrane-bound *Toxoplasma gondii* protective antigen. Cell Rep 13, 2273–2286.
Makyio H, Ohgi M, Takei T, Takahashi S, Takatsu H, Katoh Y, Hanai A, Ueda T, Kanaho Y, Xie Y, *et al*. (2012). Structural basis for Arf6-MKLP1 complex formation on the Flemming body responsible for cytokinesis. EMBO J 31, 2590–2603.
Maxfield FR, McGraw TE (2004). Endocytic recycling. Nat Rev Mol Cell Biol 5, 121–132.
Mercier C, Dubremetz JF, Rauscher B, Lecordier L, Sibley LD, Cesbron-Delauw MF (2002). Biogenesis of nanotubular network in *Toxoplasma* parasitophorous vacuole induced by parasite proteins. Mol Biol Cell 13, 2397–2409.
Meyers JM, Prekeris R (2002). Formation of mutually exclusive Rab11 complexes with members of the family of Rab11-interacting proteins regulates Rab11 endocytic targeting and function. J Biol Chem 277, 49003–49010.
Molestina RE, El-Guendy N, Sinai AP (2008). Infection with *Toxoplasma gondii* results in dysregulation of the host cell cycle. Cell Microbiol 10, 1153–1165.
Naslavsky N, Weigert R, Donaldson JG (2004). Characterization of a nonclathrin endocytic pathway: membrane cargo and lipid requirements. Mol Biol Cell 15, 3542–3552.
Nolan SJ, Romano JD, Coppens I (2017). Host lipid droplets: an important source of lipids salvaged by the intracellular parasite *Toxoplasma gondii*. PLoS Pathog 13, e1006362.
Passos ST, Silver JS, O'Hara AC, Sehy D, Stumhofer JS, Hunter CA (2010). IL-6 promotes NK cell production of IL-17 during toxoplasmosis. J Immunol 184, 1776–1783.
Prekeris R, Klumperman J, Scheller RH (2000). A Rab11/Rip11 protein complex regulates apical membrane trafficking via recycling endosomes. Mol Cell 6, 1437–1448.
Rivera-Cuevas Y, Mayoral J, Di Cristina M, Lawrence ALE, Olafsson EB, Patel RK, Thornhill D, Waldman BS, Ono A, Sexton JZ, *et al*. (2021). *Toxoplasma gondii* exploits the host ESCRT machinery for parasite uptake of host cytosolic proteins. PLoS Pathog 17, e1010138.
Romano JD, Bano N, Coppens I (2008). New host nuclear functions are not required for the modifications of the parasitophorous vacuole of *Toxoplasma*. Cell Microbiol 10, 465–476.
Romano JD, Nolan SJ, Porter C, Ehrenman K, Hartman EJ, Hsia R, Coppens I (2017). The parasite *Toxoplasma* sequesters diverse Rab host vesicles within an intravacuolar network. J Cell Biol 216, 4235–4254.
Romano JD, Sonda S, Bergbower E, Smith ME, Coppens I (2013). *Toxoplasma gondii* salvages sphingolipids from the host Golgi through the rerouting of selected Rab vesicles to the parasitophorous vacuole. Mol Biol Cell 24, 1974–1995.
Rome ME, Beck JR, Turetzky JM, Webster P, Bradley PJ (2008). Intervacuolar transport and unique topology of GRA14, a novel dense granule protein in *Toxoplasma gondii*. Infect Immun 76, 4865–4875.
Roos DS, Donald RGK, Morrissette NS, Moulton ALC (1995). Molecular tools for genetic dissection of the protozoan parasite *Toxoplasma gondii*. Methods Cell Biol 45, 27–63.
Sayles PC, Johnson LJ (1997). Exacerbation of toxoplasmosis in neutrophil depleted mice. Nat Immun 15, 249.
Schlierf B, Fey GH, Hauber J, Hocke GM, Rosorius O (2000). Rab11b is essential for recycling of transferrin to the plasma membrane. Exp Cell Res 259, 257–265.
Schonteich E, Pilli M, Simon GC, Matern HT, Junutula JR, Sentz D, Holmes RK, Prekeris R (2007). Molecular characterization of Rab11-FIP3 binding to ARF GTPases. Eur J Cell Biol 86, 417–431.
Schweitzer JK, D'Souza-Schorey C (2002). Localization and activation of the ARF6 GTPase during cleavage furrow ingression and cytokinesis. J Biol Chem 277, 27210–27216.
Schweitzer JK, Pietrini SD, D'Souza-Schorey C (2009). ARF6-mediated endosome recycling reverses lipid accumulation defects in Niemann-Pick type C disease. PLoS One 4, e5193.
Shiba T, Koga H, Hye-won S, Ryuichi K, Kazuhisa N, Soichi W (2006). Structural basis for Rab11-dependent membrane recruitment of a family of Rab11-interacting protein 3 (FIP3)/arfophilin-1. Proc Natl Acad Sci USA 103, 15416–15421.

Shin OH, Ross AH, Mihai I, Exton JH (1999). Identification of arfophilin, a target protein for GTP-bound class II ADP-ribosylation factors. J Biol Chem 274, 36609–36615.
Shin OH, Couvillon AD, Exton JH (2001). Arfophilin is a common target of both class II and class III ADP-ribosylation factors. Biochemistry 40, 10846–10852.
Sibley LD, Adams LB, Fukutomi Y, Krahenbhul JL (1991). Tumor necrosis factor alpha triggers antitoxoplasmal activity in gamma interferon primed macrophages. J Immunol 147, 2350–2355.
Sibley LD, Niesman IR, Parmley SF, Cesbron-Delauw MF (1995). Regulated secretion of multi-lamellar vesicles leads to formation of a tubulo-vesicular network in host-cell vacuoles occupied by *Toxoplasma gondii*. J Cell Sci 108, 1669–1677.
Silvis MR, Bertrand CA, Ameen N, Golin-Bisello F, Butterworth MB, Frizzell RA, Bradbury NA (2009). Rab11b regulates the apical recycling of the cystic fibrosis transmembrane conductance regulator in polarized intestinal epithelial cells. Mol Biol Cell 20, 2337–2350.
Sugawara K, Shibasaki T, Mizoguchi A, Saito T, Seino S (2009). Rab11 and its effector Rip11 participate in regulation of insulin granule exocytosis. Genes Cells 14, 445–456.
Swierzy IJ, Lüder CGK (2015). Withdrawal of skeletal muscle cells from cell cycle progression triggers differentiation of *Toxoplasma gondii* towards the bradyzoite stage. Cell Microbiol 17, 2–17.
Van Acker T, Tavernier J, Peelman F (2019). The small GTPase Arf6: an overview of its mechanisms of action and of its role in host–pathogen interactions and innate immunity. Int J Mol Sci 20, 2209.
Velásquez ZD, Conejeros I, Larrazabal C, Kerner K, Hermosilla C, Taubert A (2019). *Toxoplasma gondii*-induced host cellular cell cycle dysregulation is linked to chromosome missegregation and cytokinesis failure in primary endothelial host cells. Sci Rep 9, 12496.
Walker ME, Hjort EE, Smith SS, Tripathi A, Hornick JE, Hinchcliffe EH, Archer W, Hager KM (2008). *Toxoplasma gondii* actively remodels the microtubule network in host cells. Microbes Infect 10, 1440–1449.
Wallace DM, Lindsay AJ, Hendrick AG, McCaffrey MW (2002). Rab11-FIP4 interacts with Rab11 in a GTP-dependent manner and its overexpression condenses the Rab11 positive compartment in HeLa cells. Biochem Biophys Res Commun 299, 770–779.
Wang Z, Edwards JG, Riley N, Provance DW Jr, Karcher R, Li XD, Davison IG, Ikebe M, Mercer JA, Kauer JA, Ehlers MD (2008). Myosin Vb mobilizes recycling endosomes and AMPA receptors for postsynaptic plasticity. Cell 135, 535–548.
Wei J, Fain S, Harrison C, Feig LA, Baleja JD (2006). Molecular dissection of Rab11 binding from coiled-coil formation in the Rab11-FIP2 C-terminal domain. Biochemistry 45, 6826–6834.
Welsh GI, Leney SE, Lloyd-Lewis B, Wherlock M, Lindsay AJ, McCaffrey MW, Tavare JM (2007). Rip11 is a Rab11- and AS160-RabGAP-binding protein required for insulin-stimulated glucose uptake in adipocytes. J Cell Sci 120, 4197–4208.
Welz T, Wellbourne-Wood J, Eugen Kerkhoff E (2014). Orchestration of cell surface proteins by Rab11. Trends Cell Biol 24, 407–415.
Wilson GM, Fielding AB, Simon GC, Yu X, Andrews PD, Hames RS, Frey AM, Peden AA, Gould GW, Prekeris R (2005). The FIP3-Rab11 protein complex regulates recycling endosome targeting to the cleavage furrow during late cytokinesis. Mol Biol Cell 16, 849–860.
Wolf M, Delgado MB, Jones SA, Dewald B, Clark-Lewis I, Baggiolini M (1998). Granulocyte chemotactic protein 2 acts via both IL-8 receptors, CXCR1 and CXCR2. Eur J Immunol 28, 164–170.
Yoon SO, Shin S, Mercurio AM (2005). Hypoxia stimulates carcinoma invasion by stabilizing microtubules and promoting the Rab11 trafficking of the α6β4 integrin. Cancer Res 65, 2761–2769.
Zare-Bidaki M, Hakimi H, Abdollahi SH, Zainodini N, Arababadi MK, Kennedy D (2014). TLR4 in toxoplasmosis; friends or foe? Microb Pathog 69–70, 28–32.
Zerial M, McBride H (2001). Rab proteins as membrane organizers. Nat Rev Mol Cell Biol 2, 107–117.